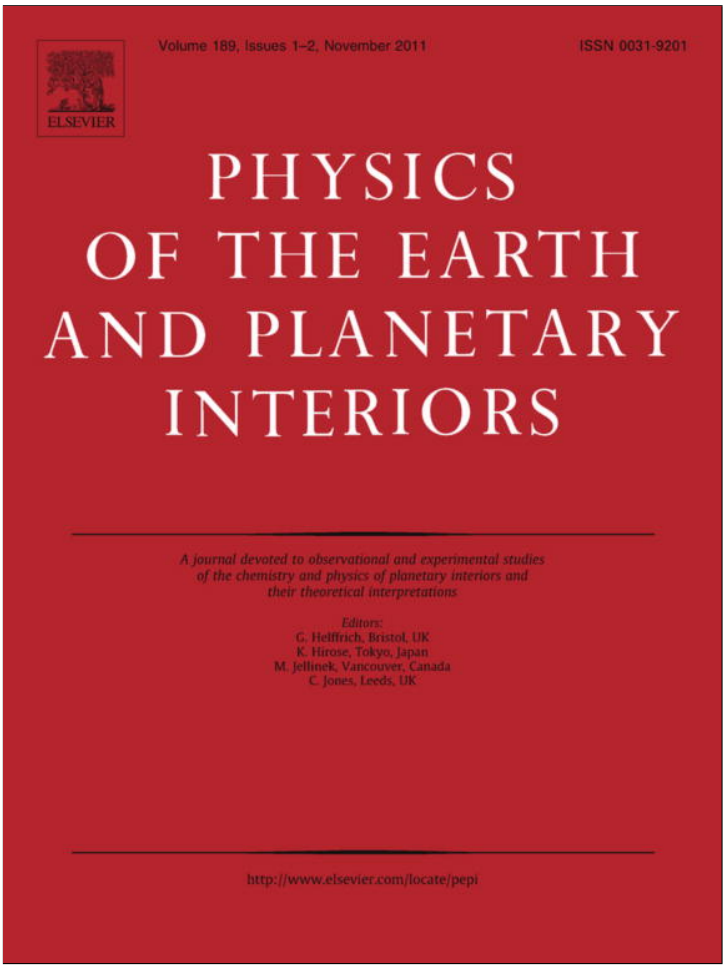

Physics of the Earth and Planetary Interiors 189 (2011) 63–79

Contents lists available at ScienceDirect

Physics of the Earth and Planetary Interiors

journal homepage: www.elsevier.com/locate/pepi

The influence of degree-1 mantle heterogeneity on the past dynamo of Mars

Hagay Amit [a,*], Ulrich R. Christensen [b], Benoit Langlais [a]

[a] CNRS UMR 6112, Université de Nantes, Laboratoire de Planétologie et de Géodynamique, 2 Rue de la Houssinière, Nantes F-44000, France
[b] Max-Planck-Institut für Sonnensystemforschung, 37191 Katlenburg-Lindau, Germany

ARTICLE INFO

Article history:
Received 3 November 2010
Received in revised form 30 June 2011
Accepted 13 July 2011
Available online 23 July 2011
Edited by Keke Zhang

Keywords:
Magnetic field
Dynamo
Mars
Hemispheric dichotomy
Mantle heterogeneity
Core–mantle boundary heat flux

ABSTRACT

The hemispheric dichotomy in the crustal magnetic field of Mars may indicate that the planet's past dynamo was influenced by a degree-1 heterogeneity on the outer boundary of its liquid metallic convecting core. Here we use numerical dynamos driven by purely volumetric internal heating with imposed degree-1 heat flux heterogeneities to study mantle control on the past dynamo of Mars. We quantify both south–north and east–west magnetic field dichotomies from time-average properties that are calculated according to two different end member crust formation scenarios. Our results indicate that a moderate heat flux anomaly may have been sufficient for obtaining the observed dichotomy. Because of the excitation of a strong equatorial upwelling in the dynamo, the efficiency of a mantle heterogeneity centered at the geographical pole in producing a south–north dichotomy is much higher than that of an heterogeneity centered at the equator in producing an east–west dichotomy. These results argue against a significant True Polar Wander event with major planet re-orientation after the cessation of the dynamo.

1. Introduction

The existence of an intrinsic magnetic field on Mars was debated until 1997, when the NASA mission Mars Global Surveyor (MGS) was inserted into orbit. At an altitude of 400 km, the Martian magnetic field components measured by MGS (Acuña et al., 2001) vary between ±250 nT, and at a lower altitude of 200 km they vary between ±650 nT. This drastic increase indicates a crustal nature to the Martian magnetic field, in contrast to Earth's anomalous crustal field which comes in excess or in deficit of the main core field. The only plausible cause for the crustal field is remanent magnetization acquired in the global field of a now extinct Martian dynamo. The largest anomalies are located south of the crustal topographic dichotomy. To first order, the northern plains, the largest volcanoes, and the largest impact craters are devoid of significant magnetic signatures.

Models that try to explain the dichotomy in the Martian crustal magnetic field fall into two categories, which we call here 'external' and 'internal'. In the external models, it is assumed that originally the entire Martian crust had been magnetized by a homogeneous internal dynamo. Later, when the dynamo had ceased to operate, parts of the magnetized crust were altered or removed by external processes such as large impacts or volcanic activity. For example, Milbury and Schubert (2010) assume that the original Martian crust had been magnetized by an internal dipole field, and that later the whole Northern hemisphere, the Tharsis volcanic province and several large impact basins are demagnetized. Their model is correlated with the Martian crustal field, but only at low spherical harmonic degrees, which contain little power. The correlation at degrees two and three requires a paleopole position at low- or mid-latitudes. While demagnetization of the crust in large impact basins seems plausible, a catastrophic event that demagnetized the entire Northern hemisphere seems less likely (Roberts and Zhong, 2006) although not impossible (Andrews-Hanna et al., 2008; Marinova et al., 2008; Nimmo et al., 2008). Large basin-forming impacts have also been invoked as cause for the sudden cessation of the paleo dynamo by reducing the core–mantle boundary (CMB) heat flux (Roberts et al., 2009) or by shock-heating the outer core leading to a stable thermal stratification (Arkani-Hamed and Olson, 2010).

The internal scenario for explaining the magnetic dichotomy assumes that the Martian crust was magnetized in a globally uneven way by a dynamo that was more active in the Southern hemisphere than in the Northern hemisphere. Even for homogeneous boundary conditions, hemispheric dynamos were found in numerical models (Grote and Busse, 2000; Simitev and Busse, 2005) for certain combinations of control parameters. In this case the selection of the magnetically active hemisphere is arbitrary and may flip in time. A degree-one thermal heterogeneity of the lower mantle could favor hemispheric dynamos in a broader range of control parameters and fix the magnetic activity to a preferred hemisphere (Stanley et al., 2008).

There are several possible causes for a hemispheric difference in the lower mantle. The intense volcanism in the region of Tharsis, together with strong gravity and topography signals there, suggest

* Corresponding author.
E-mail address: Hagay.Amit@univ-nantes.fr (H. Amit).

0031-9201/$ - see front matter © 2011 Elsevier B.V. All rights reserved.
doi:10.1016/j.pepi.2011.07.008

one-plume mantle convection upwelling below Tharsis (Zuber, 2001). Furthermore, experiments show that the Spinel to Perovskite transition may occur in the lowermost mantle of Mars (Fei et al., 1995). Harder and Christensen (1996) modeled mantle convection with such endothermic phase transition in the lowermost mantle and showed that one-plume convection emerges. Roberts and Zhong (2006) proposed that layered viscosity in the Martian mantle may lead to a degree-1 convection. Alternatively, a giant impact pre-dating the magnetization of the crust by a dynamo might have created the topographic dichotomy at the surface and set up a persistent degree one convection pattern in the mantle (Schubert et al., 2000).

Following the hypothesis of a degree-one mantle dichotomy, Stanley et al. (2008) imposed an inhomogeneous heat flux pattern with a component of spherical harmonic degree one and order zero (Y_1^0) on the outer boundary of their numerical dynamo simulation. The amplitude of the heat flux variation exceeded the mean, which means that in most of the Northern hemisphere the superadiabatic part of the CMB heat flux was assumed to be negative (inward). They found a strong south–north magnetic field dichotomy in snapshots of the magnetic field in their model. Remaining questions include:

- Can the observed dichotomy magnitude be obtained with a more moderate CMB heat flux anomaly?
- Can the dichotomy be recovered systematically in time-average field properties, corresponding to different crust formation scenarios?
- Since the mantle convection pattern was not necessarily axisymmetric with respect to the geographical pole, can a south–north dichotomy be produced if the axis of the mantle dichotomy is located at an arbitrary (e.g. mid-) latitude?

In this paper we address these issues by studying numerical dynamos driven by purely thermal convection with an imposed degree-1 heat flux heterogeneity on the outer boundary. We use heat flux anomalies of moderate amplitude corresponding to positive (outward) superadiabatic heat flux on the whole boundary. We examine Y_1^0 and Y_1^1 heat flux patterns and a combination of both. We calculate time-average field properties and their associated hemispheric dichotomies in north–south and east–west directions.

2. Current and past Martian magnetic field dichotomy

2.1. Current magnetic dichotomy

In order to quantify the degree of dichotomy of the Martian magnetic field we use the model by Langlais et al. (2004). At any given location above Mars' surface, the magnetic field is the sum of all Equivalent Source Dipole (ESD) contributions located within a certain distance. Using low- and high-altitude MGS measurements, a global map of the Martian magnetic field at altitude 400 km was produced. The horizontal resolution of the model is 170 km, or 2.9° at the equator.

Fig. 1 shows the model of the current Martian crustal magnetic field intensity B at a height of 400 km above the planet's surface (Langlais et al., 2004). According to this model, the rms of the current field intensity B in the Southern hemisphere is 29.5 nT, while the rms field in the Northern hemisphere is 8.4 nT, giving an hemispheric dichotomy ratio of 3.5. However, accounting for $\pm\sqrt{3}$ nT uncertainty in each hemisphere may give the range

$$B_{sh}/B_{nh} = 2.7 - 4.7 \quad (1)$$

for the current magnetic field hemispheric dichotomy. When searching for an hypothetical geographical pole location that yields maximal dichotomy, we obtain a dichotomy factor of 3.55 at (150°*E*, 85°*S*). This ratio is only slightly larger than the actual value and the deviation from the geographical pole is only 5°, proving that the orientation of the current dichotomy is nearly perfectly south–north.

2.2. Crustal thickness dichotomy

The Martian crust is thicker in the Southern hemisphere than in the Northern hemisphere, which may possibly explain part of the magnetic dichotomy. The thickness of the magnetized crust is controlled by the depth of the Curie temperature, i.e. the depth at which magnetic minerals lose their magnetic remanence, with the total crustal thickness as an upper bound. The Curie depth depends on the mineralogy (phase and composition), the surface temperature and the temperature gradient at Noachian time when the Martian dynamo operated.

The Curie temperature is mineral-dependent. Typical values are about 325 °C for pyrrhotite, 580 °C for pure magnetite and 670 °C for pure hematite. The Martian magnetic mineralogy is very poorly constrained (Dunlop and Arkani-Hamed, 2005). Magnetite, however, is an appealing candidate, because it possesses both a high Curie temperature and a large magnetization saturation. It occurs on Earth in both continental and oceanic crust as a primary or secondary mineral (Langlais et al., 2010). On Mars, magnetite has been detected by Spirit, on the plains and in the Columbia Hills of Gusev crater, a ~150 km-diameter crater south of Apollinaris Patera (Morris et al., 2006).

Current surface temperatures at Mars' surface are well constrained, ranging about −100 to 0 °C with an average value of −63 °C. Past temperatures can be partially constrained through the minerals that formed during the Noachian. The presence of kaolinite as observed at the surface of Mars implies that surface temperatures were likely in the 0–30 °C interval (Ehlmann et al., 2009). This is also consistent with the formation of valley networks at Noachian times, which requires the sustainability of liquid water for relatively long time intervals (Boulay et al., 2010).

The temperature profile in the Martian crust during the Noachian can be estimated indirectly from the thickness of the elastic crust, assuming a given temperature at its base. To a first order, the depth of the elastic layer is determined by the 650 °C-isotherm, beneath which the crust cannot support stresses over long intervals. Williams et al. (2008) studied the admittance, a transfer function between topography and gravity, to infer the effective elastic thickness for various parts of the Tharsis complex. The oldest parts are associated with the lowest values of the elastic thickness. Namely, the topography of the Thaumasia Highlands reflects an elastic thickness of about 20 km at the time of loading. Other studies found very similar values for all the Noachian age structures (Zuber et al., 2000; McGovern et al., 2004). Grott et al. (2007) investigated the deformation associated with two fault systems in the southern Thaumasia region. They concluded that the thermal gradient was between 17 and 32 K/km during the late Noachian to early Hesperian period. Ruiz (2009) further assumed different crustal heat production rates and found temperature gradients varying between 14.5 and 18.0 K/km depending on the estimated past surface temperature during the Noachian. Another approach consists in estimating the temperature gradient from evolution models. Choblet and Sotin (2001) assumed a stagnant lid regime for Mars' thermal evolution and concluded that the temperature gradient rapidly decreased from 30 K/km after accretion down to 8 K/km after 500 My of evolution.

Here we make the following assumptions. Noachian temperatures were on average 0 °C. Single domain magnetite is the most likely magnetic carrier and implies a Curie temperature of 580 °C. The temperature gradient ranges between 15 and 30 K/km, which implies a depth to the Curie temperature between 20 and 40 km.

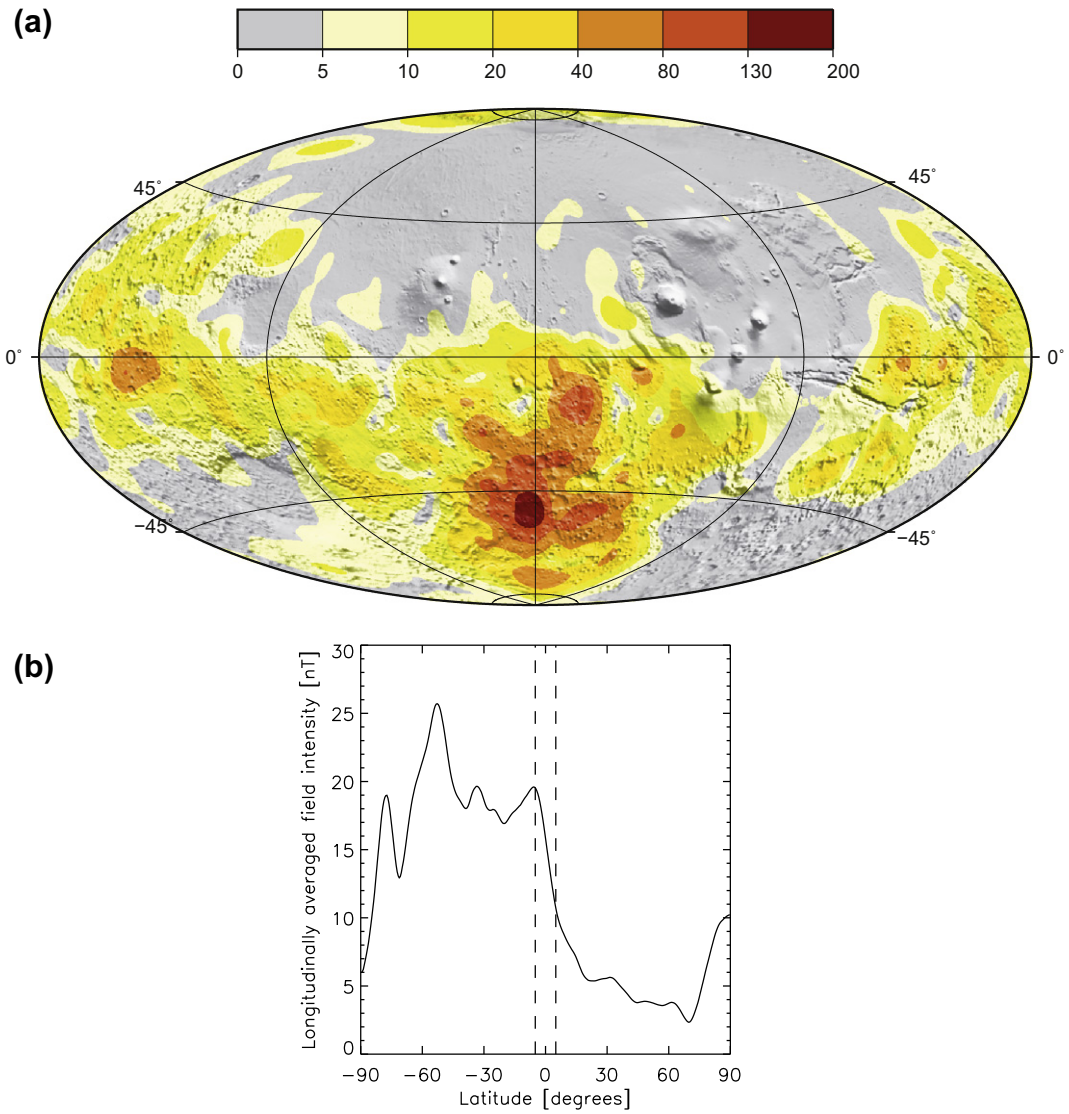

Fig. 1. (a) Current Martian crustal magnetic field intensity B at an altitude of 400 km in nT (colors) plotted over surface topography; (b) The zonal profile of the longitudinally averaged field intensity. Dashed vertical lines in (b) denote ±5° low-latitudes.

This range is compared to the 35 km thickness of the northern plains as estimated by Zuber et al. (2000). The lowest bound of the thermal gradient therefore implies that the magnetic crust would be 40 km in the Southern hemisphere vs. 35 km in the Northern hemisphere, yielding a very mild crustal thickness hemispheric dichotomy of $H_{sh}/H_{nh} \sim 1.15$, while the highest bound implies a thinner magnetic crust everywhere without any difference between the northern and southern plains, i.e. $H_{sh}/H_{nh} = 1$. In conclusion, the contribution of crustal thickness variations to the magnetic dichotomy should be relatively minor.

2.3. Past magnetic dichotomy

The current magnetic field B can be approximated as the product of the current vertically integrated magnetization M and the magnetic crustal thickness H:

$$B \propto M \cdot H \tag{2}$$

We are interested in comparing the magnitude of the past field between the two hemispheres. In the absence of later modifications, the current magnetization is directly proportional to the past one, $M \propto M_p$. It has been postulated that the Northern and Southern hemispheres were similar in age (Frey, 2006), and that the dichotomy formed during the Noachian (Milbury et al., 2007). Therefore, one can relate the current magnetic field and magnetization of Mars to the past magnetic field B_p in both hemispheres, assuming that any events that later destroyed magnetization affected both hemispheres in statistically the same way. We therefore write

$$B_p \propto M \propto B/H \tag{3}$$

Combining the range 2.7–4.7 for the current field hemispheric ratio Eq. (1) and the range 1–1.15 for the magnetic crustal thickness hemispheric ratio, we estimate the range of plausible hemispheric dichotomy of the past Martian paleomagnetic field as

$$B_{p_{sh}}/B_{p_{nh}} \sim 2.4\text{–}4.7 \tag{4}$$

2.4. Simulated magnetic dichotomy

We analyze the magnetic field output from numerical dynamo simulations, upward continued from the CMB to the Martian surface (for details see next section). We calculate the models' time-average south–north and east–west surface magnetic field intensity dichotomies. The latter is defined with respect to the phase

of the imposed Y_1^1 heat flux pattern. We assume a core radius of $r_o = 1700$ km and a surface radius of $a = 3389.5$ km.

We consider two end member crust formation scenarios (Langlais and Thébault, 2011). In the case of continuous homogeneous crust formation, each part of the Martian crust is formed by a large number of incremental additions (e.g. lava flows, sills, dykes) over an extended period of time. Each new layer would record the magnetic field at its time of formation and the present crustal field at a specific location is obtained from the vector superposition of the magnetizations of the various layers. The present local field would thus represent the intensity of a long-term time-average Martian paleomagnetic field $|\langle\vec{B}\rangle|$ (where $\vec{B}$ is the magnetic field vector and $\langle\ \rangle$ denotes time-average). In the other end-member model (random crust formation), entire crustal units were formed in relatively rapid events (with a duration short compared to the time between possible polarity reversals). Individual crustal blocks are here created randomly in space and time and each block would acquire a homogeneous magnetization recording the dynamo field at the time of formation. The characteristic crustal field strength of a large region (e.g. a hemisphere) that consists of many such blocks would reflect the time-average of the dynamo field intensity $\langle|\vec{B}|\rangle$. The two considered quantities are conceptually different. For example, for a reversing dynamo the long-term time-average field is expected to vanish, i.e. $|\langle\vec{B}\rangle|$ is zero, whereas the intensity at any snapshot is positive by definition, so $\langle|\vec{B}|\rangle$ is also positive. The actual way in which the magnetized part of the Martian crust formed may be intermediate between the two scenarios.

In the context of the continuous homogeneous crust formation scenario, we calculate the intensity of the time-average field at the planet surface $|\langle\vec{B}\rangle|$. We then calculate a surface integral hemispheric ratio, for example,

$$SN_{cnt}^{rms} = [|\langle\vec{B}\rangle|]_{sh}/[|\langle\vec{B}\rangle|]_{nh} \tag{5}$$

where SN denotes the ratio between the southern and Northern hemispheres, the subscript 'cnt' denotes *continuous* crust formation and the superscript 'rms' denotes *rms* surface average in the respective hemisphere. An alternative statistical approach considers the ratio of maximum of the zonal profile at the intense hemisphere to the maximum of the zonal profile at the other hemisphere,

$$SN_{cnt}^{zon} = max([|\langle\vec{B}\rangle|]_{sh}^{z})/max([|\langle\vec{B}\rangle|]_{nh}^{z}) \tag{6}$$

where the superscript 'zon' denotes *zonal* average. For the observed Martian crustal field (Fig. 1b), the zonal average intensity have hemispheric maxima of 25.7 nT in latitude 52.8 °S and 15.5 nT in latitude 0.3 °N, giving a ratio of $SN^{zon} = 1.7$. This value is probably not very meaningful, because the Northern hemisphere peak is right on the equator and is therefore in practice the slope of the Southern hemisphere strong field bulk. Excluding a band around the equator between 5 °N and 5 °S, we obtain a maxima ratio of $SN^{zon} = 2.4$.

In the context of the random crust formation scenario, we calculate the magnetic dichotomies based on the time-average of the magnetic field intensity $\langle|\vec{B}|\rangle$

$$SN_{rnd}^{rms} = [\langle|\vec{B}|\rangle]_{sh}/[\langle|\vec{B}|\rangle]_{nh} \tag{7}$$

$$SN_{rnd}^{zon} = max([\langle|\vec{B}|\rangle]_{sh}^{z})/max([\langle|\vec{B}|\rangle]_{nh}^{z}) \tag{8}$$

where the subscript 'rnd' denotes *random*. Eqs. (5)–(8) can be applied for the east–west dichotomies EW_{cnt}^{rms}, EW_{cnt}^{mer}, EW_{rnd}^{rms} and EW_{rnd}^{mer} by replacing the summations with the appropriate hemispheres and replacing the zonal profiles with *meridional* profiles (the latter denoted by superscript 'mer').

In addition, we wish to compare with observations not only hemispheric dichotomy ratios, but also the absolute field intensity. Analysis of the Martian meteorite ALH84001 allows a glimpse at the intensity of the Martian paleomagnetic field at the planet's surface (Weiss et al., 2002). Although largely uncertain, these estimates (assuming thermoremanent origin) range between 0.1 and 1 times Earth's present surface field intensity. The intensity of the surface geomagnetic field is about 50,000 nT, so for Mars the range is 5000–50,000 nT.

3. Numerical dynamo models

It is probable that Mars had no solid inner core up to the present day and that the early Martian dynamo was purely thermally driven, by secular cooling and perhaps by radioactive heating. For numerical reasons we retain an inner core in our dynamo models with a radius of 0.35 and 0.2 of the core radius, respectively. We make the inner core passive by imposing a zero heat flux at its boundary. Model results by Aubert et al. (2009) and Hori et al. (2010) suggest that such passive inner core with 0.35 or less of the core radius has little effect on the dynamo.

We solve the following set of self-consistent non-dimensional Boussinesq magnetohydrodynamics equations for dynamo action due to thermal convection of an electrically conducting fluid in a rotating spherical shell (e.g. Olson et al., 1999):

$$E\left(\frac{\partial\vec{u}}{\partial t} + \vec{u}\cdot\nabla\vec{u} - \nabla^2\vec{u}\right) + 2\hat{z}\times\vec{u} + \nabla P = Ra\frac{\vec{r}}{r_o}T + \frac{1}{Pm}(\nabla\times\vec{B})\times\vec{B} \tag{9}$$

$$\frac{\partial\vec{B}}{\partial t} = \nabla\times(\vec{u}\times\vec{B}) + \frac{1}{Pm}\nabla^2\vec{B} \tag{10}$$

$$\frac{\partial T}{\partial t} + \vec{u}\cdot\nabla T = \frac{1}{Pr}\nabla^2 T + \epsilon \tag{11}$$

$$\nabla\cdot\vec{u} = 0 \tag{12}$$

$$\nabla\cdot\vec{B} = 0 \tag{13}$$

where $\vec{u}$ is the velocity, $\vec{B}$ is the magnetic field, T is temperature, t is time, $\hat{z}$ is a unit vector in the direction of the rotation axis, P is pressure, $\vec{r}$ is the position vector, r_o is the core radius and ϵ is heat source. Four non-dimensional parameters in Eq. (9)–(13) control the dynamo action. The heat flux Rayleigh number (Olson and Christensen, 2002) represents the strength of buoyancy force driving the convection relative to retarding forces

$$Ra = \frac{\alpha g_0 q_0 D^4}{k\kappa\nu} \tag{14}$$

where α is thermal expansivity, g_0 is gravitational acceleration on the outer boundary at radius r_o, q_0 is the mean heat flux across the outer boundary, D is shell thickness, k is thermal conductivity, κ is thermal diffusivity and ν is kinematic viscosity. The Ekman number represents the ratio of viscous and Coriolis forces

$$E = \frac{\nu}{\Omega D^2} \tag{15}$$

The Prandtl number is the ratio of kinematic viscosity to thermal diffusivity

$$Pr = \frac{\nu}{\kappa} \tag{16}$$

and the magnetic Prandtl number is the ratio of kinematic viscosity to magnetic diffusivity λ

$$Pm = \frac{\nu}{\lambda} \tag{17}$$

We use the code MAGIC by Wicht (2002). We analyze numerical dynamos with rigid insulating boundary conditions. The models differ in the imposed outer boundary heat flux pattern and the amplitude of its variation. To study the geometrical impact of the inner-core, we compare cases with an Earth-like inner–outer core radii ra-

tio of $r_i/r_o = 0.35$ and a smaller ratio of $r_i/r_o = 0.2$. A summary of model parameters, outer boundary heat flux patterns and geometries is given in Table 1.

In all cases a volumetric homogeneous heat source ϵ compensates for the loss of heat through the outer boundary according to

$$-4\pi r_o^2 Pr\left[\frac{\partial T}{\partial r}(r_o)\right] = \frac{4}{3}\pi(r_o^3 - r_i^3)\epsilon \tag{18}$$

where $[\ldots]$ denotes averaging over the outer boundary surface S. In terms of the non-dimensional variables $\left[\frac{\partial T}{\partial r}(r_o)\right] = 1$, so for $r_i/r_o = 0.35$ the non-dimensional source term is $\epsilon \simeq 2.04$, and for $r_i/r_o = 0.2$ the source term is $\epsilon \simeq 2.42$.

Most dynamo models fall into two categories according to the principal properties of the magnetic field that they generate. In the first, the radial field on the CMB is dominated by an axial dipole component, but the field shows no tendency to ever reverse. In the second, the field is multipolar and frequent dipole reversals occur (Kutzner and Christensen, 2002). The sharp transition between the two types is probably related to a threshold value for the relative contribution of inertial effects (Christensen and Aubert, 2006; Olson and Christensen, 2006; Sreenivasan and Jones, 2006). Earth-like models that are both dipole-dominated and reversing are only found in a fairly narrow transition region between the two regimes (Olson, 2007; Wicht et al., 2009). In our study we consider cases from both regimes. As in many other dynamo model studies, we are unable to explore the control parameter space in a comprehensive way. However, because in our set of models both dynamo regimes are represented, other combinations of control parameters not explored in this study would probably not result in magnetic field solutions fundamentally different from those presented here.

Our dynamo models with $E = 3 \times 10^{-4}$ are non-dipolar and reversing. At this Ekman number we did not find dipole-dominated dynamos for the employed mode of driving convection by internal heating. The gradual decrease of Ra resulted in models with seemingly stable dipolar magnetic fields, but after more than one magnetic diffusion time the magnetic field in the dynamos dropped to very small values. In some cases the dynamo "woke up" again (sustained rise of magnetic energy), so it is not conclusive whether the dynamo exists or not. However, during the period of very low magnetic energy the field reverses, so no stable polarity dynamos were found for $E = 3 \times 10^{-4}$. However, at a lower Ekman number of $E = 1 \times 10^{-4}$, we found non-reversing dipole-dominated dynamos (Table 1).

Due to numerical singularity problems at the very center of the Earth, we cannot run our simulations with no inner core at all. We mimic the convective effect of no inner core by imposing zero buoyancy flux across the inner core. The inner core tangent cylinder is likely to determine the latitude at which intense flux patches will be concentrated on the CMB. However, at the planetary surface these structures are spread, and the impact of the inner core radius on the intensity of the field at Mars' surface is secondary. Moreover, Aubert et al. (2009) found that when keeping the convective power fixed, varying the inner core radius does not affect the main power law relations found in numerical dynamos with Earth-like inner core radius. The inner core size is important for dynamos heated from below (Heimpel et al., 2005), but for dynamos driven by internal heating it has a minor influence on the field geometry (Hori et al., 2010). We therefore conclude that the presence of an inner core in our models does not affect the main results of this study.

4. Results

4.1. Core field vs. surface field

We illustrate the results of some of our models by comparing snapshots of the radial magnetic field at the core–mantle boundary and at the surface of Mars. The sensitivity kernels of the radial and horizontal field components at a planetary radius a to the radial field at the CMB radius r_o (Gubbins and Roberts, 1983; Bloxham et al., 1989) are plotted in Fig. 2 for the assumed Martian geometry (for formulae and a more detailed discussion see (Gubbins (2004)). The two kernels depend only on the angle α between points on the planetary surface and on the CMB. The radial kernel peaks at $\alpha = 0$ (for all r_o/a ratios), i.e. the radial field at a point at the planetary surface is most strongly affected by the radial field at the CMB directly below it. Effectively, the radial kernel averages over a cap region on the CMB, with the kernel having about half its peak value at an angular distance of 30°. The horizontal kernel is zero for $\alpha = 0$ and reaches a maximum at $\alpha \sim 25°$. Overall, the field at a given point on the surface of Mars will depend mostly on the magnetic flux at the CMB in a cap of about 45° radius centered below that point.

In Fig. 3 we show two arbitrary snapshots from a model in the non-dipolar regime with a strong imposed equatorial (Y_1^1) heat flux anomaly (case 10 in Table 1). The instantaneous relations between

Table 1
Summary of numerical dynamo models. Control parameters are defined in the text. In all cases $Pr = 1$ and $Pm = 3$. The magnitude of the heat flux anomaly imposed on the outer boundary q^* is defined as the ratio of the peak-to-peak amplitude to twice the mean heat flux (Olson and Christensen, 2002). The imposed CMB heat flux patterns are either homogeneous ('hom'), degree-1 single harmonics (Y_1^0 or Y_1^1) or degree-1 inclined by 45° with respect to the rotation axis given by $Y_1^0 + Y_1^1/\sqrt{2}$. Rm is the magnetic Reynolds number based on the rms velocity. The rms value of the intensity of the time-average field on the surface of Mars is $|\langle\vec{B}\rangle|$, and the rms value of the time-average of the magnetic field intensity on the surface of Mars is $\langle|\vec{B}|\rangle$. The ratio of the time-average poloidal to toroidal magnetic energy densities in the volume E_m^p/E_m^t is also given. All magnetic field values are given in units of $\sqrt{\rho\mu_0\lambda\Omega}$ where ρ is the fluid density and μ_0 is permeability of free space. The last column 'Rev' denotes whether the model reversed or not.

Case	Pattern	q^*	r_o/r_i	E	Ra	Rm	$\lvert\langle\vec{B}\rangle\rvert$	$\langle\lvert\vec{B}\rvert\rangle$	E_m^p/E_m^t	Rev?
1	hom	0	0.35	3×10^{-4}	1.5×10^{7}	379	0.001	0.017	0.81	yes
2	hom	0	0.2	3×10^{-4}	3×10^{7}	370	0.001	0.011	0.83	yes
3	hom	0	0.2	1×10^{-4}	1×10^{7}	104	0.122	0.124	1.08	no
4	Y_1^0	0.5	0.35	3×10^{-4}	1.5×10^{7}	494	0.0003	0.006	0.53	yes
5	Y_1^0	0.8	0.35	3×10^{-4}	1.5×10^{7}	526	0.0003	0.008	0.38	yes
6	Y_1^0	0.8	0.2	3×10^{-4}	3×10^{7}	488	0.0004	0.008	0.44	yes
7	Y_1^0	0.3	0.2	1×10^{-4}	1×10^{7}	114	0.108	0.110	0.56	no
8	Y_1^0	0.5	0.2	1×10^{-4}	1×10^{7}	157	0.021	0.022	0.27	no
9	Y_1^1	0.8	0.35	3×10^{-4}	1.5×10^{7}	408	0.001	0.023	0.66	yes
10	Y_1^1	0.8	0.2	3×10^{-4}	3×10^{7}	405	0.002	0.015	0.71	yes
11	Y_1^1	0.3	0.2	1×10^{-4}	1×10^{7}	123	0.089	0.090	0.97	no
12	Y_1^1	0.5	0.2	1×10^{-4}	1×10^{7}	133	0.068	0.069	0.91	no
13	$Y_1^0 + Y_1^1/\sqrt{2}$	0.5	0.2	1×10^{-4}	1×10^{7}	139	0.044	0.045	0.43	no

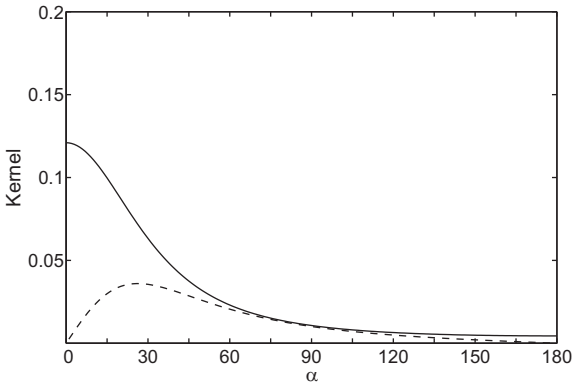

Fig. 2. Vertical (solid) and horizontal (dashed) kernels as a function of the angular distance α (in degrees) between points on the planetary surface and on the CMB, for Martian geometry, i.e. $r_o/a = 0.5$.

the radial field at the CMB, the radial field at the surface of Mars and the magnetic field intensity at the surface of Mars are shown. Note the difference in contour levels; the field at the planetary surface is weaker by a factor of order 200 compared to the CMB field. The kernels help to understand the difference between the CMB field and the surface field. Because in this small-scale multipolar dynamo model patches of both polarities are found within the effective averaging cap at the CMB for virtually every surface point, the surface intensity is weak. The field intensity is dominated by the unsigned radial field. In this case with a Y_1^1 boundary condition, the radial field on the CMB (Fig. 3a and d) is often characterized by intense flux patches of both polarities in the hemisphere of the positive heat flux anomaly (center of the maps in Fig. 3). The surface intensity (Fig. 3c and f) does not show a pronounced correlation with the heat flux maximum on the equator; relatively high intensity is found more typically at higher latitudes. Nevertheless, the strongest surface intensity in the equatorial belt appears at the longitude of the heat flux maximum in both snapshots, especially in Fig. 3f where the intensity of the equatorial structure is comparable to that of the high-latitude features.

Fig. 3 illustrates the importance of using time-average properties to accurately quantify the magnetic field dichotomies. The strongly time-dependent dynamo may produce small-scale radial field on the CMB with little correlation between one snapshot to another (Olson and Christensen, 2002; Aubert et al., 2007). Although the spatial scales are significantly larger at the Martian surface, differences between one snapshot to another may still

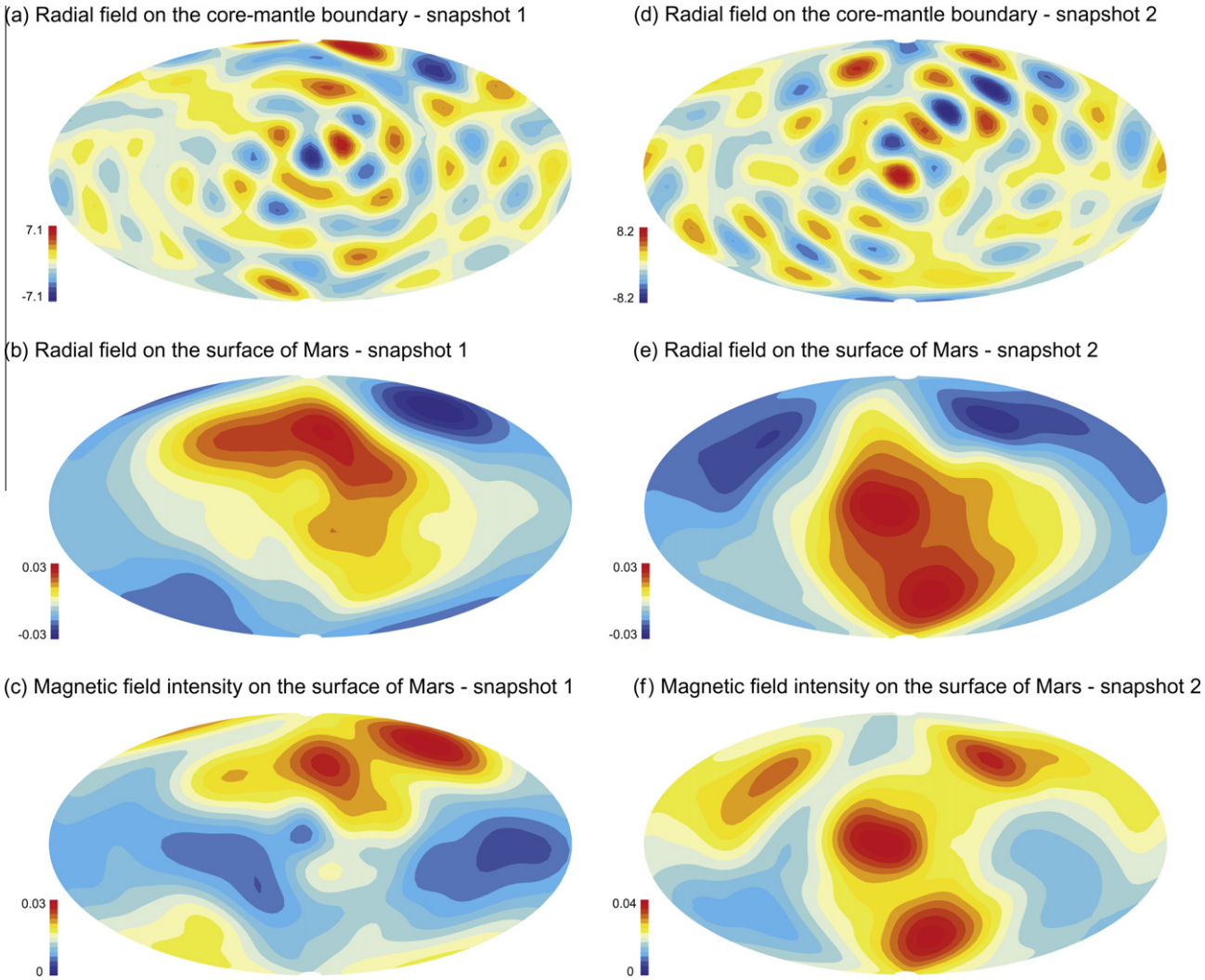

Fig. 3. Magnetic field images of two arbitrary snapshots (left column is one snapshot, right column another snapshot) from case 10: Radial field on the CMB (a and d); Radial field on the surface of Mars (b and e); Magnetic field intensity on the surface of Mars (c and f). Note that in a, b, d and e blue is negative, while in c and f the minimum value (deepest blue) is zero. The magnetic field is given in units of $\sqrt{\rho\mu_0\lambda\Omega}$. (For interpretation of the references in colour in this figure legend, the reader is referred to the web version of this article.)

appear, including different hemispheric dichotomies. For example, Fig. 3f shows some east–west dichotomy (as expected from a Y_1^1 case), whereas Fig. 3c has very little longitudinal preference.

4.2. Homogeneous CMB heat flux

We begin the magnetic field dichotomy investigation by analyzing the time-average properties of the control cases with homogeneous CMB heat flux. For reversing dynamos with homogeneous boundary conditions the field should tend to zero when averaged over a very long time and the time-average unsigned flux should become perfectly zonal and symmetric about the equator; any deviations from zero time-average field or from zonal time-average unsigned flux represent residuals due to the finite averaging period in the simulation (averaging periods τ are about 1–3 magnetic diffusion times, see Table 2). In case 2 some non-zonal structure and south–north dichotomy appear in the intensity of the surface time-average magnetic field (Fig. 4a), whereas the time-average of the surface intensity is almost perfectly zonal but still contains some south–north dichotomy (Fig. 4b). The zonal profiles (Fig. 4c and d) reflect this south–north dichotomy, while the meridional profiles (Fig. 4e and f) reflect the absence of significant dichotomy in the east–west direction. Note that both south–north and east–west dichotomies are less pronounced when considering the time-average field intensity (Fig. 4d and f) rather than the intensity of the time-average field (Fig. 4c and e).

The intensity of the time-average field is more than a factor of ten weaker than the time-average field intensity. For an infinite averaging time, the former is expected to vanish. The residual and its north–south dichotomy reflect the limited averaging time of ∼3 magnetic diffusion times (∼280 kyrs in geological time). The north–south dichotomies for the time-average field intensity of 0.98 (based on rms) and of 0.82 (based on zonal maxima) are also a result of the finite averaging time (which is probably much shorter than the time over which the Martian crust formed in whatever scenario) and conveys an idea on the typical uncertainty of the hemispheric dichotomy resulting from the limited run time of our models.

In the dipole-dominated non-reversing case 3, the time-average radial magnetic field (Fig. 5a) and the time-average unsigned flux (Fig. 5b) on the CMB are large scale and dominated by the axial dipole. The time-averaging period is still insufficient to produce a purely axisymmetric pattern on the CMB. Nevertheless, the intensity of the surface time-average magnetic field (Fig. 5c) and the time-average of the surface intensity (Fig. 5d) are converged to almost perfectly zonal and equatorially symmetric patterns, as expected. The zonal and meridional profiles (Fig. 5e-h) reflect very well the south–north symmetry and the east–west homogeneity. Because the magnetic field at the surface is dominated by the non-reversing axial dipole, the intensity of the time-average field and the time-average of the field intensity are hardly distinguishable in pattern and amplitude.

The differences between Figs. 4 and 5 emphasize the importance of dipolarity and reversals for the time-average properties. Non-dipolar reversing dynamos converge very slowly to their asymptotic steady state, on a time scale that is long compared to the time between reversals. This is especially true for the intensity of the time-average surface field that is expected to vanish over long-term averaging. The observed north–south asymmetry or longitudinal preference in the time-average properties must be considered as an artifact in the case of homogeneous boundary condition. In contrast, dipole-dominated non-reversing dynamos under homogeneous boundary conditions seem to reach a steady state practically free of longitudinal preference or south–north asymmetry on the CMB after several magnetic diffusion times (see e.g. Olson and Christensen, 2002). The planetary surface properties converge even faster, within a time period of ∼1–3 magnetic diffusion times which we typically used in our simulations (see Table 2). The impact of boundary conditions on the dynamo in terms of the statistics of the time-average properties is therefore easier to explore with non-reversing dipole-dominated dynamos. This is especially crucial for the surface quantities that are relevant to this study, because the dipole becomes increasingly significant when the CMB field is continued upwards.

Table 2
Summary of dichotomies in the dynamo models. *SN* and *EW* denote south–north and east–west, 'cnt' and 'rnd' subscripts denote *continuous* and *random* crust formation, 'rms' superscript denotes *rms* surface average, 'zon' superscript denotes maxima ratio of *zonal* profiles in each hemisphere, 'mer' superscript denotes maxima ratio of *meridional* profiles in the hemisphere centered at longitude 0° (center of large heat flux anomaly for cases 9–13) to the hemisphere centered at longitude 180°. τ is the averaging period in units of magnetic diffusion times.

Case	SN_{cnt}^{rms}	SN_{rnd}^{rms}	SN_{cnt}^{zon}	SN_{rnd}^{zon}	EW_{cnt}^{rms}	EW_{rnd}^{rms}	EW_{cnt}^{mer}	EW_{rnd}^{mer}	τ
1	–	1.55	–	1.75	–	–	–	–	2.82
2	–	1.01	–	0.86	–	–	–	–	2.88
3	1.00	1.00	1.00	1.00	–	–	–	–	1.25
4	–	2.47	–	5.12	–	–	–	–	1.80
5	–	2.88	–	7.32	–	–	–	–	2.09
6	–	2.54	–	7.78	–	–	–	–	1.63
7	1.16	1.16	1.72	1.74	–	–	–	–	0.86
8	1.49	1.50	3.33	3.35	–	–	–	–	1.03
9	–	0.99	–	0.99	–	1.01	–	1.03	2.76
10	–	1.01	–	1.01	–	1.14	–	1.14	1.26
11	1.00	1.00	1.00	1.00	0.93	0.93	0.98	0.98	3.23
12	1.00	1.00	1.00	1.00	1.01	1.01	1.00	1.00	3.47
13	1.32	1.32	2.38	2.41	0.97	0.97	0.97	0.97	0.81

4.3. Y_1^0 CMB heat flux

Next we examine cases with a Y_1^0 imposed CMB heat flux pattern (Fig. 6a). As in Stanley et al. (2008), the high heat flux is set to the Southern hemisphere where the Martian crustal field is strong. Fig. 7a and b show the intensity of the time-average field and the time-average intensity on the surface of Mars in the non-dipolar reversing case 5. In both maps a clear south–north dichotomy is observed, but the latter is roughly fifty times stronger and has a much more zonal structure, better reflecting the boundary pattern. As discussed above, the residual signal in the time-average field must be considered as an artifact of an insufficient averaging time. Fig. 7d and f show a much stronger signal in the Southern hemisphere with respect to the Northern, and the east–west difference is negligible, as expected for a Y_1^0 boundary pattern.

Fig. 8 shows the time-average magnetic field images for case 8 with a smaller inner core, and more importantly with a smaller Ekman number, which renders the dynamo to generate a non-reversing dominantly dipolar field. A north–south dichotomy is now found in both the intensity of the time-average surface field (Fig. 8c and e) and in the time-average of the surface field intensity (Fig. 8d and f). The field on the CMB is very strongly concentrated in the south pole region in this case (Fig. 8a and b). At the planetary surface this region of strong field is extended towards mid-latitudes by geometrical spreading, but is limited to the region south of −60 °S. No longitudinal preference is observed in the quantities corresponding to both crust formation scenarios (see Fig. 8g and h).

4.4. Inclined degree-1 CMB heat flux

In the multipolar reversing case 9 with an imposed Y_1^1 CMB heat flux pattern (Fig. 6b), intense magnetic flux patches are concentrated on the high heat flux hemisphere of the CMB, as expected (Fig. 9a and b). However, given the distribution at the CMB, the sur-

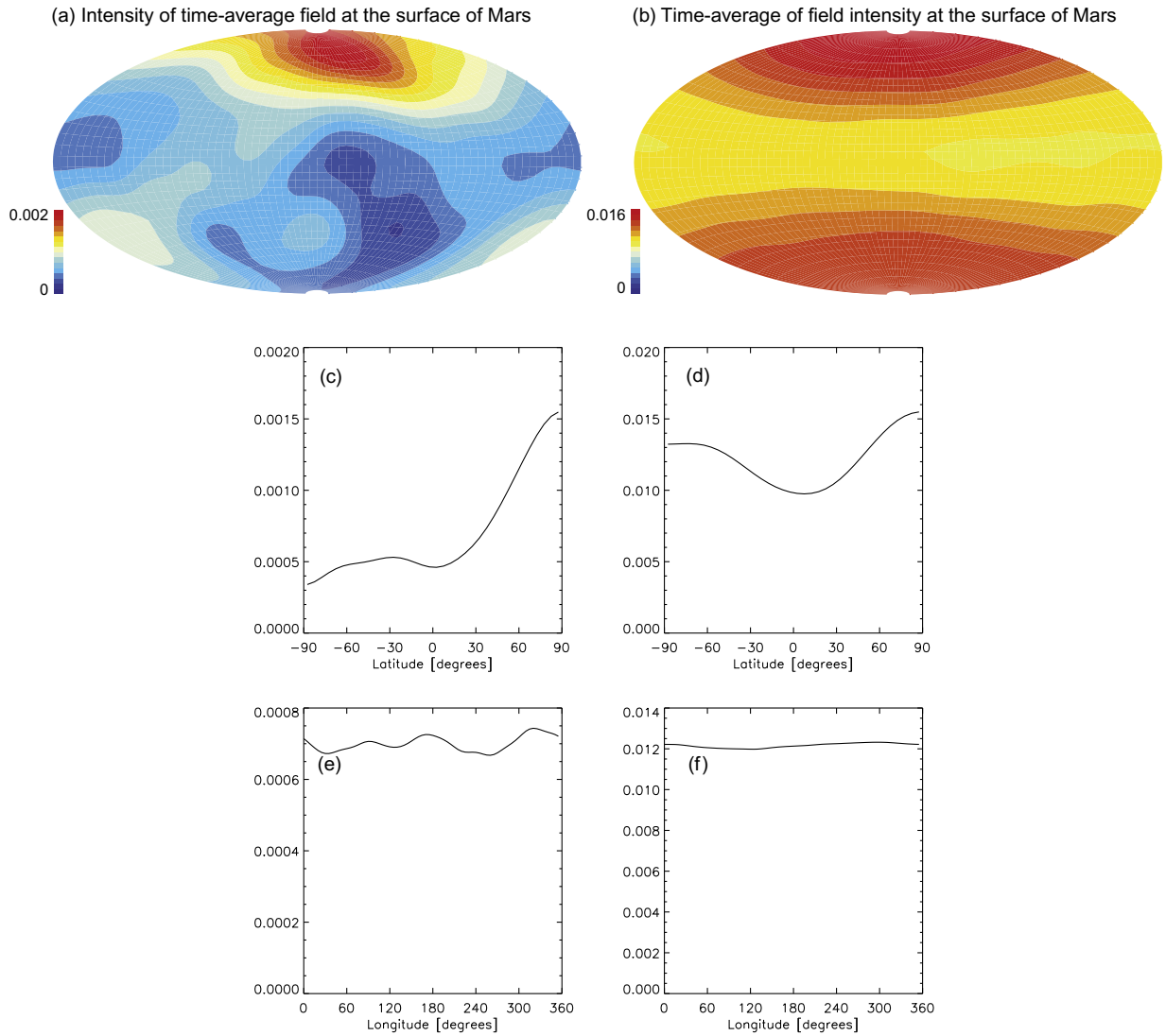

Fig. 4. Time-average magnetic field properties in case 2: (a) the intensity of the time-average magnetic field vector on Mars' surface; (b) the time-average field intensity on Mars' surface; (c) zonal profile of the intensity of the time-average field; (d) zonal profile of the time-average field intensity; (e) meridional profile of the intensity of the time-average field; (f) meridional profile of the time-average field intensity. The magnetic field is given in units of $\sqrt{\rho\mu_0\lambda\Omega}$.

face intensity patterns (Fig. 9c and d) are non-intuitive. The two quantities, $|\langle\vec{B}\rangle|$ and $\langle|\vec{B}|\rangle$, show distinctive morphologies, none of which strongly conform to a Y_1^1 pattern.

The difference between the east–west dichotomy on the CMB (Fig. 9b) to the polar-equatorial contrast on the surface (Fig. 9d) is due to the spectral content of the magnetic field in this case. The kernels in Fig. 2 show that the CMB field in a cap of roughly 45° around a point determines the surface field strength right above it. The CMB field at low latitudes, where an east–west dichotomy is apparent, is dominated by small-scales and hence strongly damped when upward continued to the surface. The radial flux emerging within a cap of ∼45° at low-latitudes averages nearly to zero. The field emerging at high latitudes, however, contains on top of the small-scale components some significant large-scale components that reach the surface. Indeed, the field maps generated from snapshots truncated to spherical harmonic degree and order 3 exhibit polar-equatorial contrasts in both CMB and surface patterns (compare Fig. 10b and d). This reasoning obviously applies only to the reversing non-dipolar dynamos; the non-reversing dipole-dominated dynamos do not have significant small-scale contributions and thus their CMB and surface magnetic field patterns are much more correlated.

Fig. 11 shows the surface magnetic field intensities for another case with Y_1^1 imposed heat flux pattern, but this time the outer core shell is thicker with $r_i/r_o = 0.2$. Note that the Y_1^1 signature in the surface intensity is sharper with respect to the thinner shell case – compare Fig. 9d with Fig. 11b, and their meridional profiles – compare Fig. 9h with Fig. 11f. Overall, the boundary effect seems to be stronger in the thicker shell case. The origin of this difference will be explored in the next section.

So far we considered cases with two extreme degree-1 heat flux patterns where the heterogeneity peak is either at the geographical pole (Y_1^0) or inclined by 90° and centered at the equator (Y_1^1). In general, however, the peak mantle heterogeneity could be at any arbitrary latitude. We finally examine the dipolar case 13 with a degree-1 heat flux heterogeneity centered at latitude 45 °S (Fig. 6c). This case produces an appreciable south–north dichotomy without any detectable east–west dichotomy. The reason for this result will also be explained in the next section.

4.5. Magnetic field strength

We next examine whether our models' magnetic field intensities are plausible in comparison with estimates of the Martian

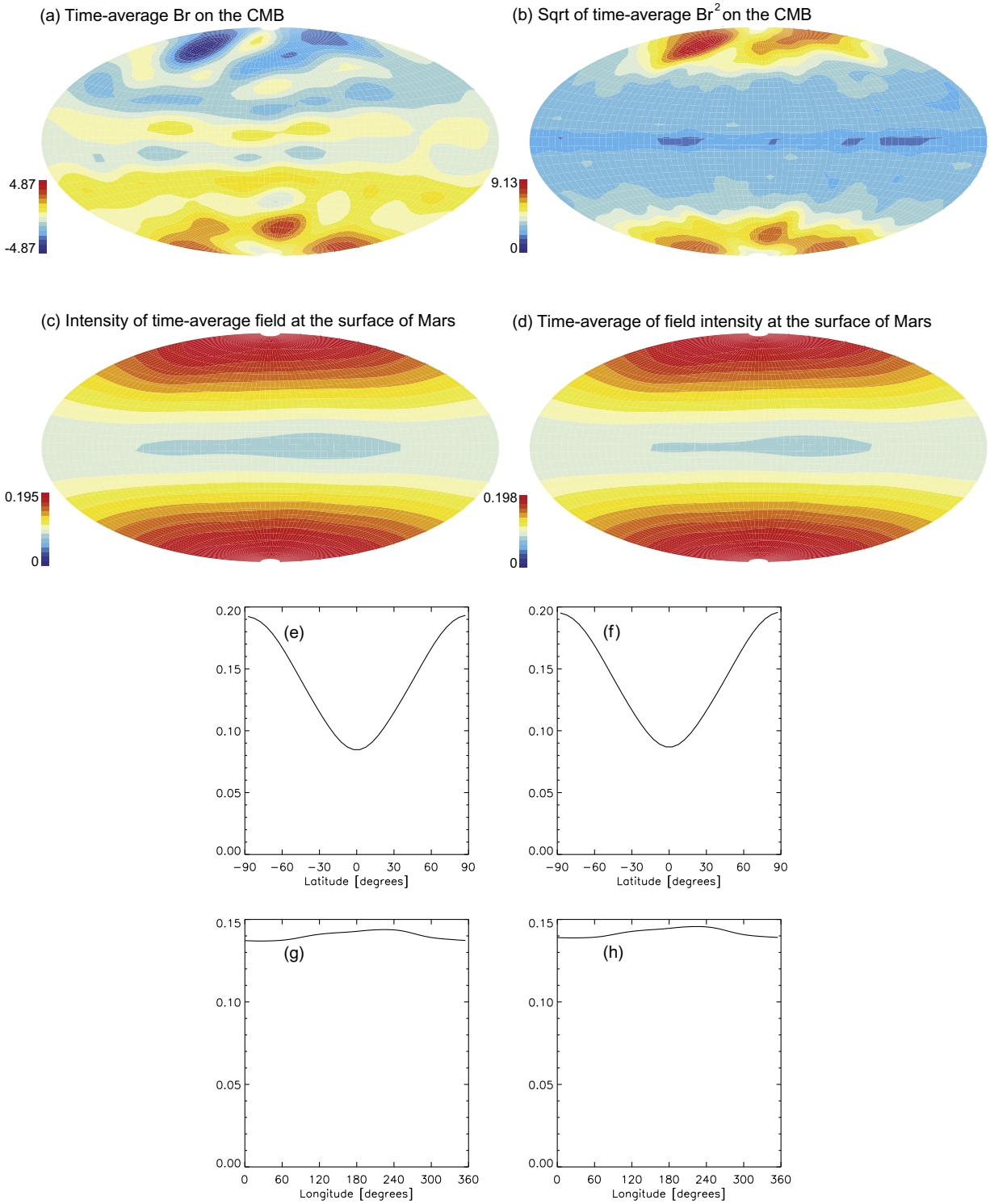

Fig. 5. Time-average magnetic field properties in case 3: (a) time-average radial field on the CMB; (b) time-average unsigned radial field on the CMB; (c) the intensity of the time-average magnetic field vector on Mars' surface; (d) the time-average field intensity on Mars' surface; (e) zonal profile of the intensity of the time-average field; (f) zonal profile of the time-average field intensity; (g) meridional profile of the intensity of the time-average field; (h) meridional profile of the time-average field intensity. The magnetic field is given in units of $\sqrt{\rho\mu_0\lambda\Omega}$.

paleomagnetic field strength. We rescale the magnetic field strength obtained in the models for the Martian surface in a straightforward way to physical units. A potential problem with this approach is that the field intensities in the model may not be directly comparable with that of the Martian field because control parameters (E, Pm, Ra) are very different from planetary values. The intensity values in Table 1 are given in units of $\sqrt{\rho\mu_0\lambda\Omega}$ where ρ is the fluid density and μ_0 is permeability of free space. Using appropriate values of $\rho = 8000\ \mathrm{kg\ m^3}$, $\lambda = 1.4\ \mathrm{m^2\ s^{-1}}$ and $\Omega = 7 \times 10^{-5}\ \mathrm{s^{-1}}$, the non-dimensional values in Table 1 can also be read as physical values in units of mT. We compare these model values to the range of 0.05–0.005 mT for Mars (Weiss et al., 2002).

In the scenario of continuous homogeneous crust formation, the intensity of the time-average surface field is relevant. In our revers-

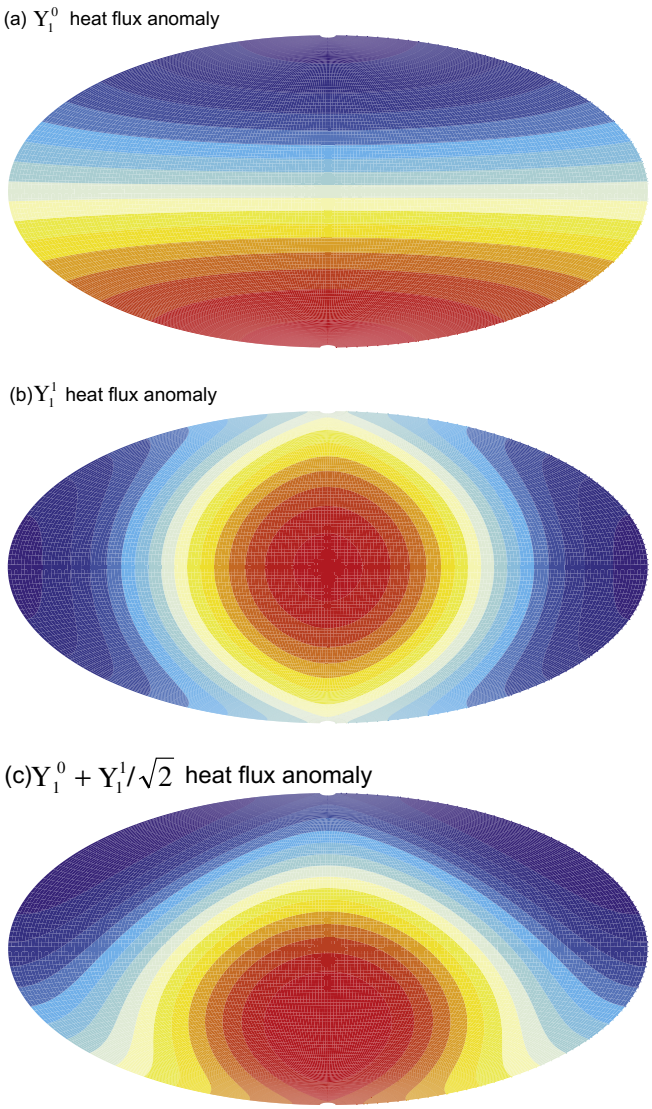

Fig. 6. Degree-1 heterogeneous heat flux patterns Y_1^0 (a), Y_1^1 (b) and $Y_1^0 + Y_1^1/\sqrt{2}$ (c). Red is positive anomalies, blue is negative. (For interpretation of the references in colour in this figure legend, the reader is referred to the web version of this article.)

ing non-dipolar cases, it is below the estimated minimum value of the magnetizing Martian surface field. The averaging time of our dynamo runs is probably much shorter than the time interval of crust formation. The average for a longer time interval is expected to be even smaller than the residual values tabulated in Table 1. If the way in which the magnetized Martian crust was formed has been similar to our continuous homogeneous scenario, a frequently reversing dynamo must be ruled out. In the random crust formation scenario, the time-average of the field intensity is relevant. It is in the plausible range for the ancient Martian field also in the case of non-dipolar reversing dynamos, although cases with a Y_1^0 heterogeneity are close to the lower bound (Table 1).

The non-reversing cases have comparable $|\langle\vec{B}\rangle|$ and $\langle|\vec{B}|\rangle$ values, which fall well in the expected range, or even above this range. Overall, the surface field magnitudes in the reversing cases are smaller than in the non-reversing cases due to the smaller scales dominating the CMB field in the reversing dynamos. Also note that increasing the degree of heterogeneity q^* increases the vigor of convection (see *Rm* values in Table 1) but decreases the surface field strength.

Because both our reversing and non-reversing dynamo models exhibit plausible intensities within the range inferred by Weiss et al. (2002), we can neither prove nor rule out the existence of reversals in the past Martian dynamo. From a dynamical point of view, the field strength inside the outer core shell scales with the convective buoyancy flux (Christensen and Aubert, 2006). The smaller core of Mars compared to the Earth would imply a larger buoyancy flux, but the purely thermal convection in Mars' core as opposed to the thermo-chemical convection in Earth's core would give an opposite effect. Comparison of fixed temperature and fixed heat flux boundary conditions in numerical dynamos driven by internal heating shows that the latter is characterized by larger convective structures and a more dipolar field (Hori et al., 2010).

4.6. Comparing field dichotomies

In the reversing non-dipolar dynamos the time-average field should approach zero in the long run, therefore we list the dichotomy in the homogeneous crust formation scenario only for the non-reversing cases (Table 2). Also, we list the values for the east–west dichotomy only for cases with a longitude-dependent heat flux distribution. In the non-dipolar control cases with homogeneous heat flux (see cases 1 and 2 in Table 2) the north–south dichotomies deviate more strongly from unity than expected, although not as strongly as non-dipolar dynamos with a strong Y_1^0 heterogeneity (cases 4–6). Obviously these dynamos can maintain a hemispheric imbalance for several magnetic diffusion times even for homogeneous boundary conditions (Landeau and Aubert, 2011). In contrast, the dipole-dominated non-reversing dynamos with homogeneous heat flux (case 3) or with a purely longitudinal heat flux variation (cases 11 and 12) show no hemispheric dichotomy.

The dipolar dynamo cases with Y_1^0 heat flux pattern (cases 7 and 8 in Table 2) show very similar values of the degree of south–north dichotomy for the two crust formation scenarios, but the values vary between the two statistical approaches. In terms of the difference in *rms* values between the two hemispheres it is rather small for a heat flux heterogeneity $q^* = 0.3$ and somewhat stronger when q^* is increased to 0.5. The hemispheric differences are more pronounced when considering the ratio of the maxima in the zonal averages in each hemisphere, where the dichotomy goes up to 3.33 in the case of $q^* = 0.5$. Comparison of cases 7 and 8 shows that the south–north dichotomies based on the zonal maxima are roughly linear with q^*. For the same amplitude of heat flux variation, $q^* = 0.5$, the non-dipolar dynamo (case 4) shows a significantly stronger hemispheric dichotomy than the dipolar dynamo (case 8).

In contrast, dynamos with a purely longitudinal (Y_1^1) distribution of heat flux (cases 9–12 in Table 2) produce only a very weak east–west dichotomy both in the dipolar and in the non-dipolar cases. Even for the highest heat flux ratio of $q^* = 0.8$ the east–west dichotomy is only 1.12. We note that for $E = 1 \times 10^{-4}$ the dynamo changes from dipolar non-reversing at lower heat flux amplitude values of up to $q^* = 0.5$ to non-dipolar reversing at $q^* = 0.8$, with all other parameters unchanged.

In the dipolar dynamo with a degree-1 heterogeneity that is inclined by 45° with respect to the rotation axis (case 13), we observe a clear south–north dichotomy, but no significant east–west dichotomy. The magnitude of the south–north dichotomy is in agreement with that of the corresponding Y_1^0 case 8 – the ratio of the SN^{zon} values (identical for both crust formation scenarios) is $2.38/3.33 = 0.71 \sim \sqrt{2}/2$, in very good agreement with the expected value from the projection of the inclined heat flux distribution onto the rotation axis.

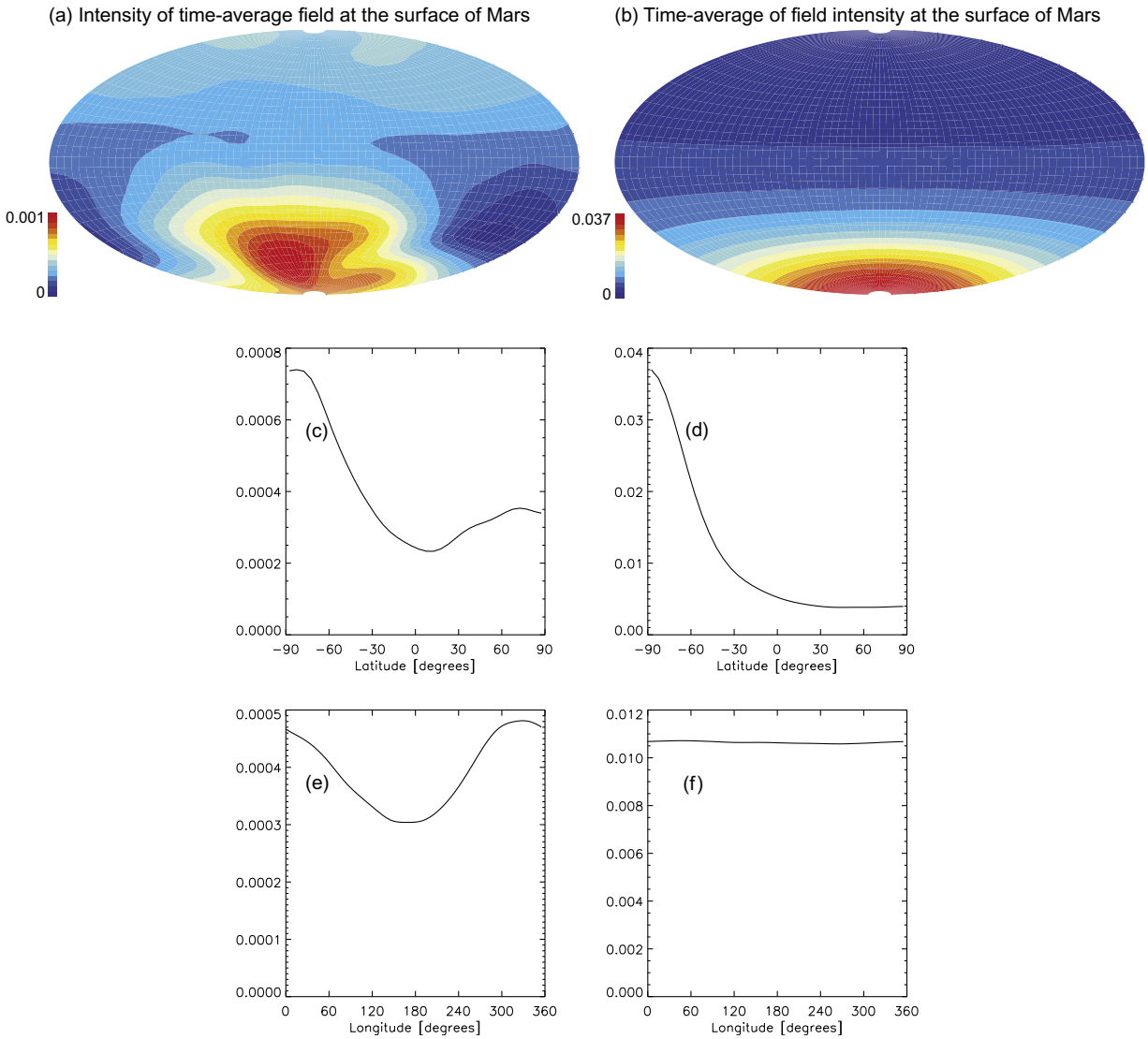

Fig. 7. As in Fig. 4 for case 5.

5. Mechanisms of magnetic dichotomy

There are two possible end member mechanisms for producing a strong north–south dichotomy in the Y_1^0 cases. In the first, convection is less vigorous in the low heat flux hemisphere, and hence magnetic field generation is also less intense in this hemisphere (Stanley et al., 2008). Alternatively, the meridional circulation changes from poleward transport in both hemispheres near the CMB in the homogeneous or equatorially symmetric heat flux cases (Figs. 12 and 13) to transport from the Northern to the Southern hemisphere for the Y_1^0 cases (e.g. Fig. 14). Indeed, the time-average meridional velocity at the top of the free stream of case 5 is 23.5 southward (in units of v/D). For comparison, the time-average azimuthal velocity of this case is -10.7 westward. The strong meridional flow transports magnetic flux that emerges in the Northern hemisphere or at low-latitudes towards the south polar cap region.

Our results suggest that the Y_1^0 boundary pattern is much more efficient in producing magnetic field dichotomy than the Y_1^1 pattern. We argue that the reason for this difference is that the background homogeneous convection in numerical dynamos is comprised of upwelling in low-latitudes (Aubert, 2005) that suppresses concentration of magnetic flux. For prescribed heat flux boundary conditions the equatorial upwelling is even stronger than for fixed temperature conditions (Sakuraba and Roberts, 2009; Hori et al., 2010). This background meridional circulation is well reflected in the time-average zonal temperature and velocity profiles. The homogeneous and Y_1^1 cases (see e.g. Figs. 12 and 13) exhibit zonal patterns of warm plumes and fluid upwelling in the equator, and cold downwelling at high-latitudes, resulting in magnetic field concentrations at high-latitudes. The Y_1^1 boundary-driven dynamics contains one longitudinal hemisphere with colder low-latitudes, but the overall background warm low-latitudes due to the homogeneous convection counteracts the cold regions and no significant downwelling is obtained, resulting in weak field concentrations and weak (if any) Y_1^1 signature in the surface magnetic field maps. In contrast, a Y_1^0 pattern produces stronger/weaker downwelling structures (see Fig. 14) and field concentrations at high-latitudes of the high/low heat flux, respectively. In this case the asymmetric boundary condition results in equatorial asymmetry of the zonal temperature and flow, and in the breaking of the Taylor–Proudman constraint (as was previously found by Stanley et al., 2008). A schematic illustration of the difference in efficiency between Y_1^0 and Y_1^1 due to the interaction with the background homogeneous upwelling pattern is given in Fig. 15.

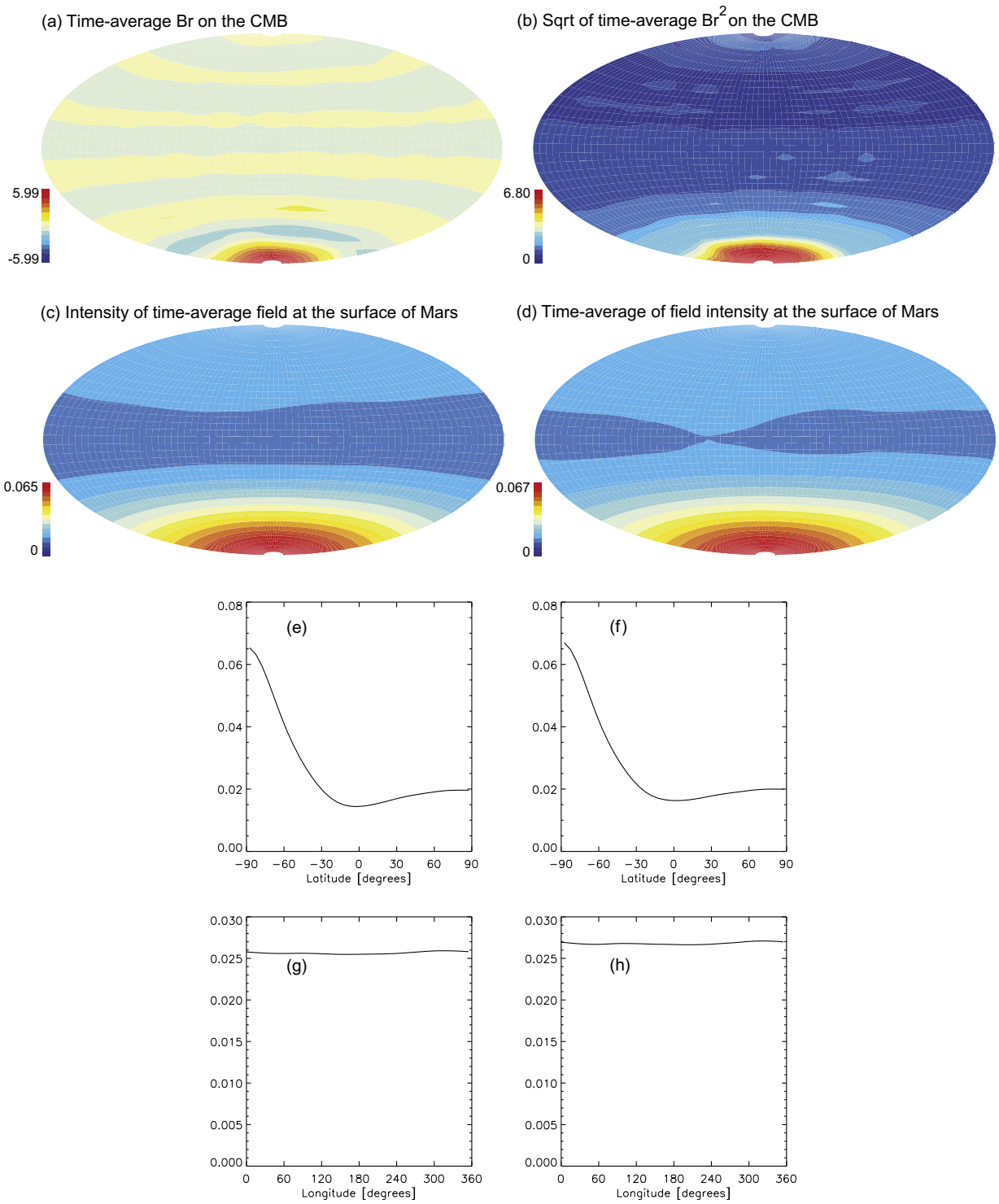

Fig. 8. As in Fig. 5 for case 8.

The dynamical differences between cases 9 and 10 that lead to the different east–west dichotomies are evident in the time-average zonal equatorial upwelling. In case 9, the time-average zonal tangential divergence $\langle \nabla_h \cdot \vec{u_h} \rangle^{zon}$ on the equator at the top of the free stream is 20.8 and 7.5 (in units of v/D^2) in the low/high heat flux hemispheres, respectively, whereas in case 10 the corresponding values are 37.8 and −10.6. The overall positive equatorial upwelling in case 9 diminishes the possibility for a significant east–west dichotomy, whereas in case 10 the boundary-driven flow is strong enough to counteract the background homogeneous dynamo equatorial upwelling and obtain some downwelling and field concentration in the colder hemisphere.

Detecting a Y_1^1 signal in the surface intensity maps therefore relies on the relative strength of the equatorial upwelling in the background homogeneous convection. For simplicity, consider that the overall downwelling is a linear sum of the background homogeneous zonal flow U_{hom} and the mantle-driven flow U_{mant}. The background flow is comprised of high-latitude downwelling

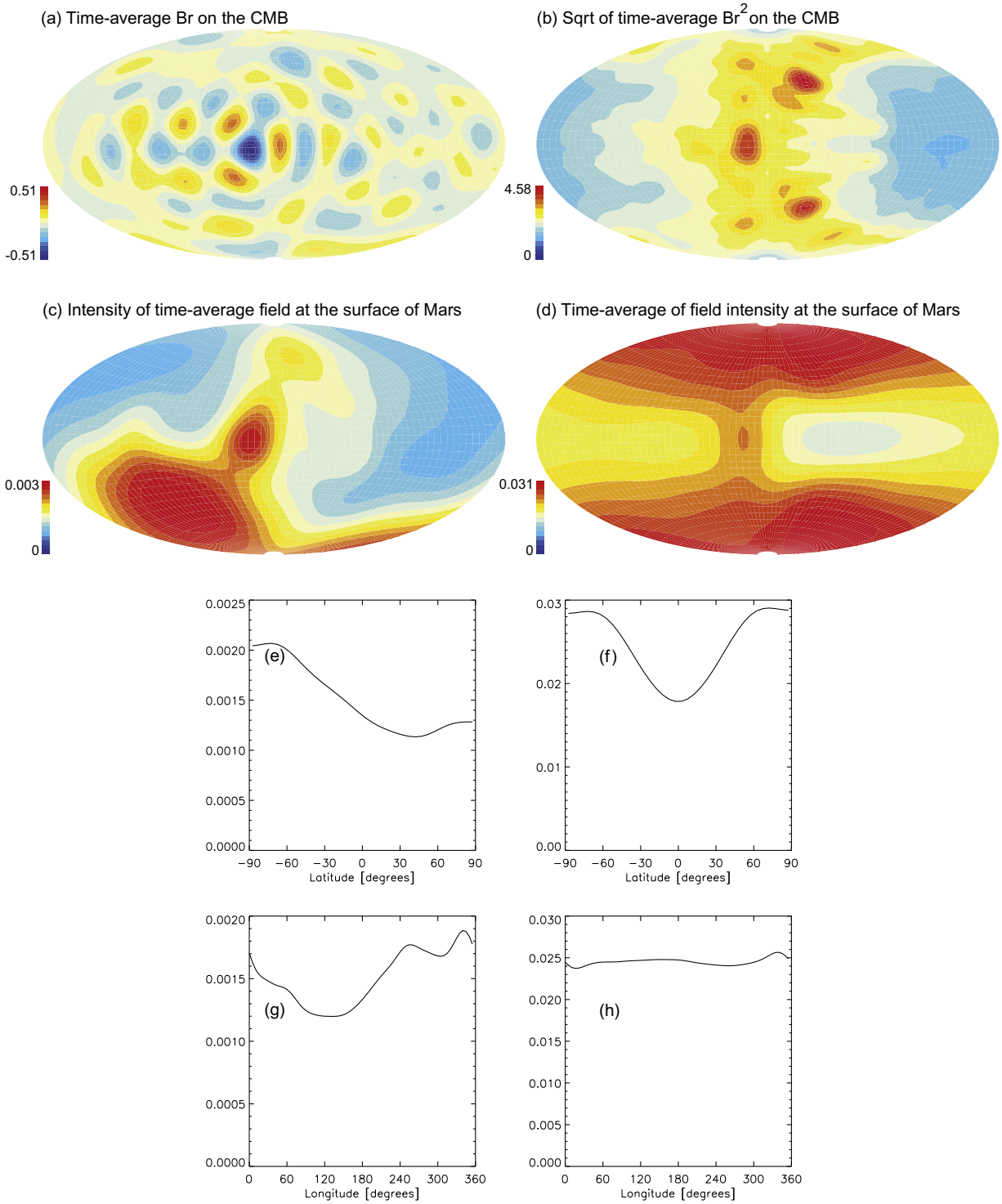

Fig. 9. As in Fig. 5 for case 9.

$U^{hl}_{hom} < 0$ and equatorial upwelling $U^{eq}_{hom} > 0$, while a Y^1_1 pattern will produce in one hemisphere some equatorial downwelling flow $U^{eq}_{mant} < 0$. Detecting the boundary effect depends on the ratio $(|U^{eq}_{mant}| - |U^{eq}_{hom}|)/|U^{hl}_{hom}|$. Because U^{eq}_{mant} depends on q^* and is comparable in the Y^1_1 cases 9 and 10, the relative detectability of the Y^1_1 signal between these two cases depends on the ratio $|U^{eq}_{hom}|/|U^{hl}_{hom}|$. Different inner core size results in different convective power (Aubert et al., 2009), so the structure of the underlying homogeneous convection is different between cases 9 and 10. When the relative importance of the homogeneous equatorial upwelling is weaker (as in case 10, see Fig. 13), the Y^1_1 effect is stronger in the surface intensity (Fig. 11d). In contrast, when the relative importance of the equatorial upwelling is stronger (as in case 9, see Fig. 12), the hemispheric equatorial downwelling is counteracted by the homogeneous equatorial upwelling, and the Y^1_1 effect in the surface intensity is weaker (Fig. 9d).

We finally note that the cases with equatorial asymmetry in the imposed heat flux pattern are characterized by lower poloidal to

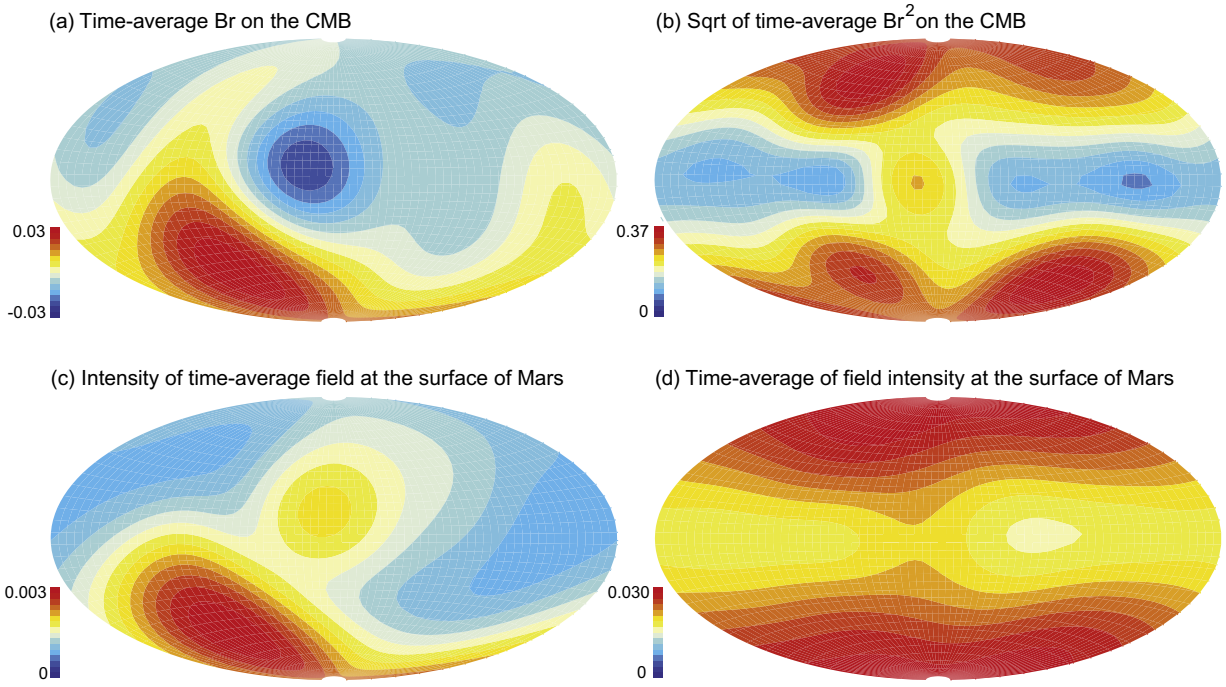

Fig. 10. As in Fig. 9a–d for the same case 9 but expanded until spherical harmonic degree $\ell_{max} = 3$ only.

toroidal magnetic energies ratios than the homogeneous and Y_1^1 cases (Table 1). Symmetry breaking in the dynamo therefore results in stronger (relative) toroidal fields generated by thermal wind shear in the shell, a smaller portion of the CMB field lines cross the surface, and weaker surface field intensity. The efficiency in producing a magnetic field dichotomy is thus counteractive to the efficiency in producing a strong surface field. Both efficiencies, however, are amplified in the presence of a more vigorous convection.

6. Discussion and conclusions

Two end-member models have been proposed to explain the north–south dichotomy of the Martian crustal magnetic field, one in which large parts of an originally homogeneously magnetized crust have been later demagnetized or removed (e.g. Milbury and Schubert, 2010), and another in which the Martian paleo dynamo lacked the hemispherical symmetry that is typical for the present geomagnetic field (Stanley et al., 2008). At present, neither scenario can be rejected and both may have contributed to some degree. In this paper we explore the second scenario in greater detail than was done before.

In order to demonstrate that heterogeneous CMB heat flux with a Y_1^0 pattern can lead to a strongly hemispheric dynamo, Stanley et al. (2008) assumed a very large amplitude of heat flux variations $q^* = 3$ in their dynamo model, which implies negative super-adiabatic heat flux in the Northern hemisphere. Our study shows that a Y_1^0 pattern with modest heterogeneities on the order of $q^* = 0.5$ with a superadiabatic heat flux everywhere is sufficient to produce a south–north magnetic field dichotomy that is within the range of observed values (Eq. 4). A systematic study of the dependence of the magnetic field dichotomy on q^* is problematic, because increasing the amplitude of the heat flux heterogeneity to $q^* = 0.8$ results in the transition from dipole-dominated non-reversing dynamos to reversing non-dipolar dynamos. Within the range of q^* values below that transition, the dependence of the dichotomy on q^* seems roughly linear. Landeau and Aubert (2011) even show that for internal heating and sufficiently vigorous convection, a hemispheric dichotomy in the flow pattern may arise spontaneously for uniform CMB heat flux. Heterogeneous heat flux would strengthen such symmetry breaking and select the preferred hemisphere for the dynamo.

We found that significantly different magnetic dichotomies may be observed from one snapshot to another. Two time-average field properties corresponding to two extreme crust formation scenarios were therefore considered. For each scenario we applied two global statistical measures. We found that the dichotomies are insensitive to the crust formation scenarios, but vary depending on the statistical approach. When using rms ratios, the low-latitudes regions where the field intensity is low reduce the dichotomy, whereas when using maxima ratios of zonal profiles, the dichotomy reflects well the difference in high-latitude field strength (where the most significant magnetic flux structures typically appear) between the two hemispheres.

Finally, while there are arguments in favor of a degree-1 mantle heterogeneity in Mars, it seems unlikely that this heterogeneity was centered exactly at the geographical pole. By comparing simulations with Y_1^0 and Y_1^1 patterns, we found that the Y_1^0 pattern is much more efficient in producing a south–north dichotomy than a Y_1^1 in producing an east–west dichotomy, due to the interaction with the background dynamo meridional circulation. Thus a degree-1 mantle heterogeneity centered at an arbitrary latitude not too close to the equator is likely to produce a detectable south–north dichotomy and a negligible east–west dichotomy, as is confirmed in the case with 45° inclination.

The last result has direct consequences for the history of mantle dynamics on Mars. It is possible to estimate the location of the magnetic paleopole, assuming that the magnetic field was that of a Mars-centered axial dipole. Some studies did not find any particular cluster for the paleopoles (e.g. Frawley and Taylor, 2004), while others concluded that paleomagnetic poles are preferentially located around the Tharsis bulge (Arkani-Hamed, 2001; Arkani-Hamed and Boutin, 2004; Hood et al., 2005; Quesnel et al.,

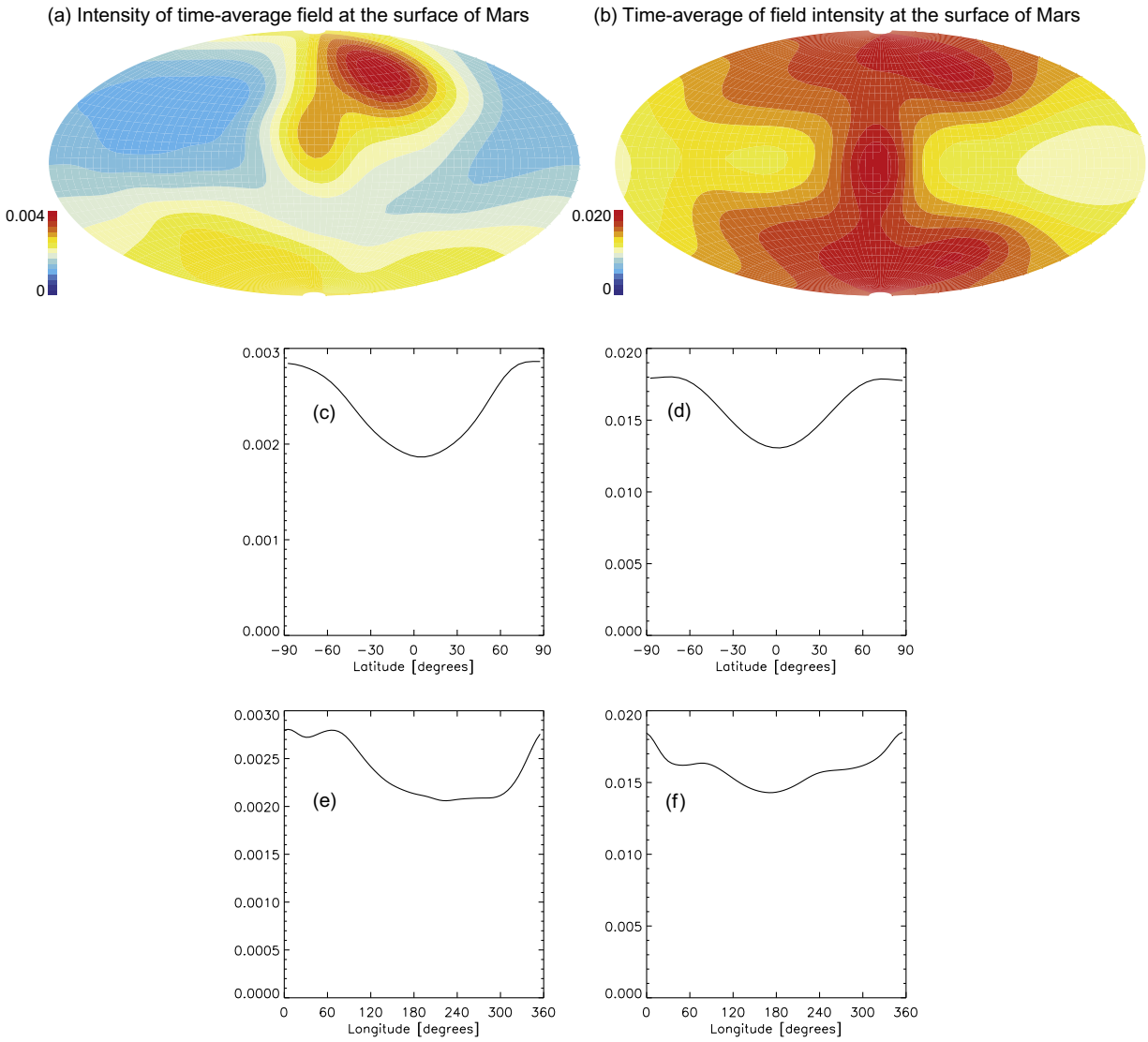

Fig. 11. As in Fig. 4 for case 10.

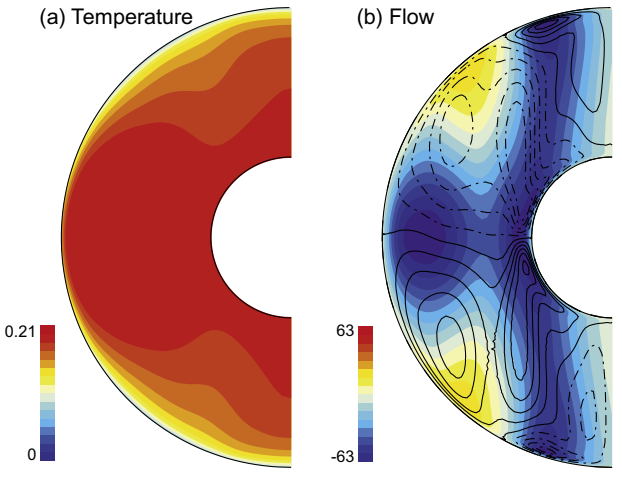

Fig. 12. Temperature (a) and velocity (b) time-average zonal profiles for case 9. The meridional streamfunction contour interval is 0.07. At the top of the free stream $|U^{eq}_{hom}|/|U^{hl}_{hom}| = 0.135$.

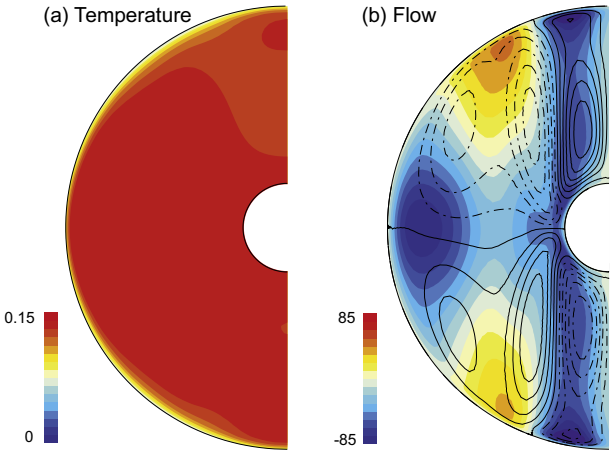

Fig. 13. As in Fig. 12 for case 10. The meridional streamfunction contour interval is 0.23. At the top of the free stream $|U^{eq}_{hom}|/|U^{hl}_{hom}| = 0.059$.

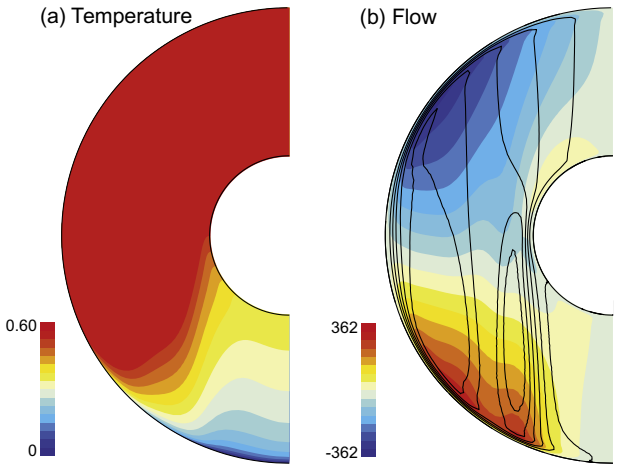

Fig. 14. As in Fig. 12 for case 5.

2007; Langlais and Quesnel, 2008), supporting the idea that a major True Polar Wander (TPW) event occurred, which re-oriented the dichotomy to its present state. Roberts and Zhong (2007) proposed that a single-plume mantle convection at an arbitrary latitude had a net positive geoid and therefore migrated to the equator. Thickened crust formed above the plume causing the geoid above it to become negative, resulting in TPW moving the crustal dichotomy to a north–south orientation, with Tharsis possibly formed on the crustal dichotomy boundary by edge-driven convection and migrated equatorward to its present location. In contrast, Daradich et al. (2008) concluded using general physical arguments supported by a fluid Love number analysis that the re-orientation of the pole associated with the development of Tharsis was likely less than 15°. Langlais and Purucker (2007) studied a magnetic anomaly associated with a late Noachian-age volcano, Apollinaris Patera. The magnetic paleopole that they found is located at the current geographic pole, suggesting that a TPW, if any, occurred prior to the shutdown of the dynamo. This single result was recently confirmed by Hood et al. (2010). Our study contributes a core dynamics argument for this debate. The much higher efficiency of a Y_1^0 pattern over a Y_1^1 in our models suggests that, if the magnetic dichotomy at the surface of Mars is indeed related to a heat flux heterogeneity at the CMB, then the original dichotomy generated by the Martian paleo dynamo was oriented close to south–north, precluding a major TPW event.

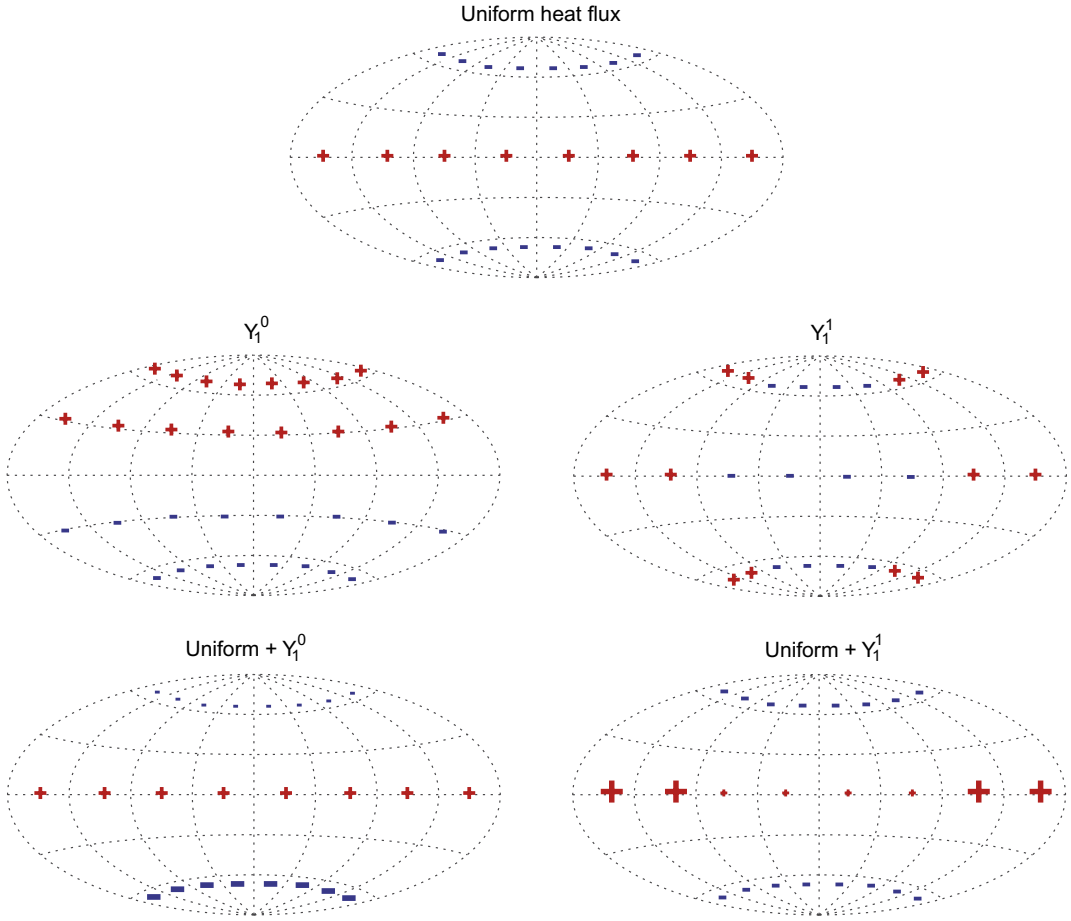

Fig. 15. Schematic illustration of the upwelling patterns induced by homogeneous and heterogeneous CMB heat flux patterns, and their superpositions. Homogeneous heat flux (top) yields high-latitude downwelling (blue minus signs) which concentrates magnetic flux, and equatorial upwelling (red plus signs) which disperses magnetic flux. Heterogeneous heat flux (middle) yields downwelling/upwelling where the heat flux is anomalously positive/negative, respectively. The superposition of the background conditions and the Y_1^0 heterogeneity (bottom left) yields weaker/stronger downwelling in the northern/southern high-latitudes, hence a south–north dichotomy in the field intensity. In contrast, the superposition of the background conditions and the Y_1^1 heterogeneity (bottom right) merely yields weaker/stronger upwelling in the eastern/western equatorial region, in both cases magnetic flux is not concentrated, and no east–west dichotomy is obtained. If the Y_1^1 boundary-driven downwelling/upwelling exceeds the homogeneous equatorial upwelling, some weak downwelling may occur in one hemisphere, resulting in some east–west dichotomy in the magnetic field. (For interpretation of the references in colour in this figure legend, the reader is referred to the web version of this article.)

Acknowledgments

H.A. and B.L. were supported by grants from the Agence Nationale de la Recherche (Project ANR-08-JCJC-0126-01) and Program PNP of the French *Institut National de Sciences de l'Univers* and CNRS. H.A. thanks the Max-Planck-Institut für Sonnensystemforschung for their generous hosting during several visits that promoted this paper. We thank Johannes Wicht for providing the MAGIC code. We thank Kumiko Hori, Wieland Dietrich and Johannes Wicht for insightful discussions.

References

Acuña, M., Connerney, J., Wasilewski, P., Lin, R., Mitchell, D., Anderson, K., Carlson, C., McFadden, J., Remè, H., Mazelle, C., Vignes, D., Bauer, S., Cloutier, P., Ness, N., 2001. Magnetic field of Mars: summary of results from the aerobraking and mapping orbits. J. Gephys. Res. 106, 23403–23417.

Andrews-Hanna, J., Zuber, M., Banerdt, W., 2008. The Borealis basin and the origin of the Martian crustal dichotomy. Nature 453, 1212–1215. doi:10.1038/nature07011.

Arkani-Hamed, J., 2001. Paleomagnetic pole positions and pole reversals of Mars. Geophys. Res. Lett. 28. doi:10.1029/2001GL012928.

Arkani-Hamed, J., Boutin, D., 2004. Paleomagnetic poles of Mars: revisited. J. Geophys. Res. 109. doi:10.1029/2003JE002229.

Arkani-Hamed, J., Olson, P., 2010. Giant impact stratification of the Martian core. Geophys. Res. Lett. 37, L02201. doi:10.1029/2009GL041417.

Aubert, J., 2005. Steady zonal flows in spherical shell fluid dynamos. J. Fluid Mech. 542, 53–67.

Aubert, J., Amit, H., Hulot, G., 2007. Detecting thermal boundary control in surface flows from numerical dynamos. Phys. Earth Planet. Inter. 160, 143–156.

Aubert, J., Labrosse, S., Poitou, C., 2009. Modelling the paleo-evolution of the geodynamo. Geophys. J. Int. 179, 1414–1428.

Bloxham, J., Gubbins, D., Jackson, A., 1989. Geomagnetic secular variation. Phil. Trans. Roy. Soc. London A329, 415–502.

Boulay, S., Cradock, R., Mangold, N., Ansan, V., 2010. Characterization of fluvial activity in Parana Valles using different age-dating techniques. Icarus 207. doi:10.1016/j.icarus.2009.12.030.

Choblet, G., Sotin, C., 2001. Early transient cooling of Mars. Geophys. Res. Lett. 28. doi:10.1029/2001GL012896.

Christensen, U., Aubert, J., 2006. Scaling properties of convection-driven dynamos in rotating spherical shells and application to planetary magnetic fields. Geophys. J. Int. 166, 97–114.

Daradich, A., Mitrovica, J., Matsuyama, I., Perron, J., Manga, M., Richards, M., 2008. Equilibrium rotational stability and figure of Mars. Icarus 194, 463–475.

Dunlop, D., Arkani-Hamed, J., 2005. Magnetic minerals in the Martian crust. J. Geophys. Res. 110. doi:10.1029/2005JE002404.

Ehlmann, B., Mustard, J., Swayze, G., Clark, R., Bishop, J., Poulet, F., Des Marais, D., Roach, L., Milliken, R., Wray, J., Barnouin-Jha, O., Murchie, S., 2009. Identification of hydrated silicate minerals on Mars using MRO-CRISM: geologic context near Nili Fossae and implications for aqueous alteration. J. Geophys. Res 114. doi:10.1029/2009JE003339.

Fei, Y., Prewitt, C., Mao, H.-K., Bertka, C., 1995. Structure and density of FeS at high pressure and high temperature and the internal structure of Mars. Science 268, 1892–1894.

Frawley, J., Taylor, P., 2004. Paleo-pole positions from Martian magnetic anomaly data. Icarus 172, 316–327.

Frey, H., 2006. Impact constraints on the age and origin of the lowlands of Mars. Geophys. Res. Lett. 33. doi:10.1029/2005GL024484.

Grote, E., Busse, F., 2000. Hemispherical dynamos generated by convection in rotating spherical shells. Phys. Rev. E 62, 4457–4460.

Grott, M., Hauber, E., Werner, S., Kronberg, P., Neukum, G., 2007. Mechanical modeling of thrust faults in the Thaumasia region, Mars, and implications for the Noachian heat flux. Icarus 186. doi:10.1016/j.icarus.2006.10.001.

Gubbins, D., 2004. Time Series Analysis and Inverse Theory for Geophysicists. Cambridge University Press, Cambridge, UK.

Gubbins, D., Roberts, N., 1983. Use of the frozen-flux approximation in the interpretation of archaeomagnetic and paleomagnetic data. Geophys. J.R. Astr. Soc. 73, 675–687.

Harder, H., Christensen, U., 1996. A one-plume model of Martian mantle convection. Nature 380, 507–509.

Heimpel, M., Aurnou, J., Al-Shamali, F., Gomez Perez, N., 2005. A numerical study of dynamo action as a function of spherical shell geometry. Earth Planet. Sci. Lett. 236, 542–557.

Hood, L., Harrison, K., Langlais, B., Lillis, R., Poulet, F., Williams, D., 2010. Magnetic anomalies near Apollinaris Patera and the Medusae Fossae formation in Lucus Planum, Mars. Icarus 208, 118–131. doi:10.1016/j.icarus.2010.01.009.

Hood, L., Young, C., Richmond, N., Harrison, K., 2005. Modeling of major Martian magnetic anomalies: further evidence for polar reorientations during the Noachian. Icarus 177. doi:10.1016/j.icarus.2005.02.008.

Hori, K., Wicht, J., Christensen, U., 2010. The effect of thermal boundary conditions on dynamos driven by internal heating. Phys. Earth Planet. Inter. 182, 85–97. doi:10.1016/j.pepi.2010.06.011.

Kutzner, C., Christensen, U., 2002. From stable dipolar towards reversing numerical dynamos. Phys. Earth Planet. Inter. 131, 29–45.

Landeau, M., Aubert, J., 2011. Equatorially antisymmetric convection inducing a hemispherical magnetic held in rotating spheres and implications for the past Martian dynamo. Phys. Earth Planet. Inter 185, 61–73.

Langlais, B., Lesur, V., Purucker, M., Connerney, J., Mandea, M., 2010. Crustal magnetic fields of terrestrial planets. Space Sci. Rev. 152, 10.1007/s11214-009-9557-y.

Langlais, B., Purucker, M., 2007. A polar magnetic paleopole associated with Apollinaris Patera, Mars. Planet. Space Sci. 55, 270–279.

Langlais, B., Purucker, M., Mandea, M., 2004. Crustal magnetic field of Mars. J. Geophys. Res. 109, E02008.

Langlais, B., Quesnel, Y., 2008. New perspectives on Mars' crustal magnetic field. Comp. Rend. Geosci. 340. doi:10.1016/j.crte.2008.08.006e.

Langlais, B., Thébault, E., 2011. Predicted and observed magnetic signatures of Martian (de)magnetized impact craters. Icarus 212, 10.1016/j.icarus.2011.01.015.

Marinova, M., Aharonson, O., Asphaug, E., 2008. Mega-impact formation of the Mars hemispheric dichotomy. Nature 453, 1216–1219.

McGovern, P., Solomon, S., Smith, D., Zuber, M., Simons, M., Wieczorek, M., Phillips, R., Neumann, G., Aharonson, O., Head, J., 2004. Correction to Localized gravity/topography admittance and correlation spectra on Mars: implications for regional and global evolution. J. Geophys. Res. 109. doi:10.1029/2004JE002286.

Milbury, C., Schubert, G., 2010. Search for the global signature of the Martian dynamo. J. Geophys. Res. 115. doi:10.1029/2010JE003617.

Milbury, C., Smrekar, S., Raymond, C., Schubert, G., 2007. Lithospheric structure in the eastern region of Mars' dichotomy boundary. Planet. Space Sci. 55. doi:10.1016/j.pss.2006.03.009s.

Morris, R., Klingelhöfer, G., Schröder, C., Rodionov, D., Yen, A., Ming, D., de Souza, P., Fleischer, I., Wdowiak, T., Gellert, R., Bernhardt, B., Evlanov, E., Zubkov, B., Foh, J., Bonnes, U., Kankeleit, E., Gütlich, P., Renz, F., Squyres, S., Arvidson, R., 2006. Mössbauer mineralogy of rock, soil, and dust at Gusev crater, Mars: spirit's journey through weakly altered olivine basalt on the plains and pervasively altered basalt in the Columbia Hills. J. Geophys. Res. 111. doi:10.1029/2005JE002584.

Nimmo, F., Hart, S., Horycansky, D., Agnor, C., 2008. Implications of an impact origin for the Martian hemispheric dichotomy. Nature 453, 1220–1223.

Olson, P., 2007. Gravitational dynamos and the low frequency geomagnetic secular variation. Proc. Nat. Acad. Sci. 104, 20159–20166.

Olson, P., Christensen, U., 2002. The time averaged magnetic field in numerical dynamos with nonuniform boundary heat flow. Geophys. J. Int. 151, 809–823.

Olson, P., Christensen, U., 2006. Dipole moment scaling for convection-driven planetary dynamos. Earth Planet. Sci. Lett. 250, 561–571.

Olson, P., Christensen, U., Glatzmaier, G., 1999. Numerical modeling of the geodynamo: mechanisms of field generation and equilibration. J. Geophys. Res. 104, 10383–110404.

Quesnel, Y., Langlais, B., Sotin, C., 2007. Local inversion of magnetic anomalies: implication for Mars' crustal evolution. Planet. Space Sci. 55, 258–269.

Roberts, J., Lillis, R., Manga, M., 2009. Giant impacts on early Mars and the cessation of the Martian dynamo. J. Geophys. Res. 114, E04009. doi:10.1029/2008JE003287.

Roberts, J., Zhong, S., 2006. Degree-1 convection in the Martian mantle and the origin of the hemispheric dichotomy. J. Geophys. Res. 111. doi:10.1029/2005JE002668.

Roberts, J., Zhong, S., 2007. The cause for the north–south orientation of the crustal dichotomy and the equatorial location of Tharsis on Mars. Icarus 190, 24–31.

Ruiz, J., 2009. The very early thermal state of Terra Cimmeria: implications for magnetic carriers in the crust of Mars. Icarus 203. doi:10.1016/j.icarus.2009.05.021.

Sakuraba, A., Roberts, P., 2009. Generation of a strong magnetic field using uniform heat flux at the surface of the core. Nature Geosci. 2, 802–805.

Schubert, G., Russell, C., Moore, W., 2000. Timing of the Martian dynamo. Nature 408, 666–667.

Simitev, R., Busse, F., 2005. Prandtl-number dependence of convection-driven dynamos in rotating spherical fluid shells. J. Fluid Mech. 532, 365–388.

Sreenivasan, B., Jones, C., 2006. The role of inertia in the evolution of spherical dynamos. Geophys. J. Int. 164, 467–476.

Stanley, S., Elkins-Tanton, L., Zuber, M., Parmentier, E., 2008. Mars' paleomagnetic field as the result of a single-hemisphere dynamo. Science 321, 1822–1825.

Weiss, B., Vali, H., Baudenbacher, F., Kirschvink, J., Stewart, S., Shuster, D., 2002. Records of an ancient Martian magnetic field in ALH84001. Earth Planet. Sci. Lett. 201, 449–463.

Wicht, J., 2002. Inner-core conductivity in numerical dynamo simulations. Phys. Earth Planet. Inter. 132, 281–302.

Wicht, J., Stellmach, S., Harder, H., 2009. Numerical models of the geodynamo: from fundamental Cartesian models to 3D simulations of field reversals. In: Glassmeier, H., Soffel, H., Negendank, J. (Eds.), Geomagnetic Field Variations – Space-time Structure, Processes, and Effects on System Earth. Springer, Berlin.

Williams, J.-P., Nimmo, F., Moore, W., Paige, D., 2008. The formation of Tharsis on Mars: what the line-of-sight gravity is telling us. J. Geophys. Res. 113. doi:10.1029/2007JE003050.

Zuber, M., 2001. The crust and mantle of Mars. Nature 412, 220–227.

Zuber, M., Solomon, S., Phillips, R., Smith, D., Tyler, G., Aharonson, O., Balmino, G., Banerdt, W., Head, J., Johnson, C., Lemoine, F., McGovern, P., Neumann, G., Rowlands, D., Zhong, S., 2000. Internal structure and early thermal evolution of Mars from Mars Global Surveyor topography and gravity. Science 287, 1788–1793.